Probabilistic Seismic Demand of 2-D Steel Moment Resisting Frames in Estimation of Collapse under Earthquake Ground Motions

Pedram Khajehhesameddin

Submitted to the
Institute of Graduate Studies and Research
in partial fulfillment of the requirements for the Degree of

Master of Science
in
Civil Engineering

Eastern Mediterranean University
June 2010
Gazimağusa, North Cyprus

Approval of the Institute of Graduate Studies and Research

Prof. Dr. Elvan Yılmaz
Director (a)

I certify that this thesis satisfies the requirements as a thesis for the degree of Master of Science in Civil Engineering.

Prof. Dr. Ali Günyaktı
Chair (a), Department of Civil Engineering

We certify that we have read this thesis and that in our opinion it is fully adequate in scope and quality as a thesis for the degree of Master of Science in Civil Engineering.

Asst. Prof. Dr. Serhan Şensoy
Supervisor

Examining Committee

1. Asst. Prof. Dr. Erdinc Soyer
2. Asst. Prof. Dr. Giray Özay
3. Asst. Prof. Dr. Serhan Şensoy

ABSTRACT

This study concentrates on evaluation and estimation of collapse of two 3-story and 9-story steel moment resisting frames designed by SAC/ FEMA for the place of Los Angeles California. “Collapse” in this research is defined as the loss of lateral load-resisting capacity of frame structural system by the application of ground motion and by considering P-Δ effects on the dummy column. Dummy column is connected to the steel moment-resisting frame in order to consider the effects of gravity loads of the real 3-D structure while 2-D frame is extracted from 3-D frame. Estimation of collapse performance requires the relation between a ground motion intensity measures (IM) and the probability of collapse defined as collapse fragility curve as well as the relation between the same ground motion IM and the seismic hazard for the building defined as seismic hazard curve.

Among two methods of estimating the collapse fragility curve; IM-based and EDP-based, the first method is carried out in this research because of its better performance in collapse limit state according to the previous research. In this approach, collapse is associated with ground motion IM and it is obtained by using Incremental Dynamic Analysis. The collapse performance criteria that are obtained from this research are compared with the collapse performance criteria recommended by Haselton and SAC/FEMA guidlines.

Keywords: Incremental dynamic analysis, Fragility curve, Mean annual frequency, Seismic Hazard Curve, Probabilistic.

ÖZ

Bu çalışmada SAC/FEMA ilkeleri dikkate alınarak Los Angeles California bölgesi için tasarlanan 3 katlı ve 9 katlı çelik çerçeve sistemlerin göçme durumunun tahmini yapılmıştır. Bu tez çalışması kapsamında "göçme", fiktiv kolonlarda ikinci mertebe moment etkisinin de göz önüne alındığı halde bir çerçeve sistemin sismik yük altında yatay yük taşıma kapasitesini kayıbetmesi durumunu anlatmaktadır. Fiktiv kolonlar gerçek 3 boyutlu taşıyıcı sistemde düşey yük etkisinin 2 boyutlu modele yansıtılması amacı ile ana çerçeve sisteme eklenen kolonlar olarak ele alınmıştır. Göçme performansının tahmin edilmesi kırılganlık eğrisi olarak tanımlanan deprem şiddeti ile göçme olasılığı ilişkisi ve buna paralel olarak deprem şiddeti ile söz konusu bölgede bina için tanımlanan deprem tehlike eğrisinin oluşturulması ile yapılmıştır.

Göçme olasılığının tahmin edilmesi için var olan iki yöntemden şiddet ölçüsünün kullanılması özellikle göçme limit durumunda önceki çalışmalarda daha iyi sonuçlar vereceğininin belirtilmesinden dolayı bu çalışmada da kullanılmış, bir diğer yöntem olan mühendis-talep-parametrsi kullanılmamıştır. Bu çalışmada göçme durumu deprem şiddeti ile ilişkilendirilmiş ve Artımsal Dinamik Analiz yöntemiyle elde edilmiştir. Bu çalışma sonucunda elde edilen göçme performansı, Haselton ve SAC/FEMA tarafından önerilen kriterler doğrultusunda değerlendirilmiştir.

Anahtar Kelimeler: Artımsal Dinamik Analiz, Krılganlık eğrisi, ortalama yıllık frekans, Sismik Tehlike Eğrisi, olasılık.

To my family

ACKNOWLEDGMENTS

Words fail to express my deepest appreciation and gratitude to my supervisor, Asst. Prof. Dr. Serhan Şensoy, for his guidance, patience, enthusiasm and motivation throughout this study.

I would like to respect my parents, Mohammad and Ziba, whose supports are always the cause of success, happiness and self-confidence in my life. Also, I appreciate my brother and my best friend, Parham, whose dignified smile is the most beautiful thing I always eager to see.

Special thanks to my uncle, Abbaas, and aunts, Fereshteh, Zohreh and Lahya, whose emotions made the distances short in abroad, since I came to Cyprus Island.

I would like to thank all the members of Civil Engineering Department, specially Prof. Dr. Ali Günyaktı, Asst. Prof. Dr. Erdinc Soyer, Assoc. Prof. Dr. Özgür Eren, Asst. Prof. Dr. Giray Özay and Asst. Prof. Dr Huriye Bilsel for all the things I've learnt from them and for their advises and kindnesses. Also, I want to express my gratitude to Saeid Kamkar my best comrade and all of the numerous individuals who contributed to make these years at E.M.U. enjoyable and gainful.

TABLE OF CONTENTS

LIST OF TABLES

LIST OF FIGURES

LIST OF ABBREVIATIONS AND SYMBOLS

ABBREVIATIONS

ATC	Applied Technology Council
CD	Cyclic Deterioration
CUREE	Consortium of Universities for Research in Earthquake Engineering
DCF	Cumulative Distribution Function
DI	Damage Index
EDP	Engineer Demand Parameter
EQ	Earthquake
FC	Fragility Curve
FEMA	Federal Emergency Management Agency
IDA	Incremental Dynamic Analysis
IM	Intensity Measure
IM_C	Intensity Measure at Collapse State
LTB	Lateral Torsional Buckling
MAF	Mean Annual Frequency
NPT	Total Number of an EQ Record Interval Points
PEER	Pacific Earthquake Engineering Research
PGA	Peak Ground Acceleration
PGV	Peak Ground Velocity
PSHA	Probabilistic Seismic Hazard Analysis
RC	Reinforced Concrete

RTR	Record to Record
SAC	SEAOC ATC CUREE
SEAOC	Structural Engineering Association of California
SDOF	Single Degree of Freedom
SI	System International
SMRF	Steel Moment Resisting Frame
USGS	United States Geological Survey

SYMBOLS

λ_c	Mean Annual Frequency of Collapse
Δ	Displacement
P	Lateral Load

Chapter 1

INTRODUCTION

1.1 Motivation

One major purpose of seismic deign is to protect the structure against “collapse”. This general word is defined as the loss of capacity of a structure when subjected to seismic excitation. Global collapse may be the cause of dynamic instability in a side-sway mode, which is started by large story drifts and increased in amplitude by second order P-Δ effects and loss of strength and stiffness of the components of structural system.

Capability of predicting the dynamic response of deteriorating structures is almost the most significant part in the assessment of collapse, particularly for those older structures that the failure occurs at the relatively smaller deformations in comparison with the modern structures. For such systems, the global collapse is assumed to be associated with “acceptable” story drift or a “limited” value of deformation in any elements of the structural system. It is noted that these assumptions for collapse mechanism are just because of the lack of information about hysteretic models that are able to simulate failure behavior for the older constructions. The approach used in this research has the ability to consider the effects of redistributions of damage and also mentions the capacity of the system before collapse to sustain deformations larger than those that are associated with loss in the resistance of individual components.

Therefore, the approach that is integrating all the sources of global collapse of the structural systems should include the effects of strength deterioration, cyclic deterioration (CD) as well as second order P-Δ effects. In this research, global collapse occurs due to the incremental "side-sway" collapse of at least one story of the structure.

1.2 Objective

The objective of this research is to apply a methodology for prediction of global side-sway collapse performance that results the relation between a ground motion intensity measure (IM) and the probability of collapse known as "collapse fragility curve" as well as the relation between that ground motion intensity measures and the seismic hazard for the building, known as "seismic hazard curve".

The approach applied for predicting the collapse fragility curve of a structure is name as IM-based approach in which, collapse is obtained by Incremental Dynamic Analysis (IDA).

Two 3-Story and 9-story Steel Moment Resisting Frames (SMRF) are analyzed to obtain the estimates of collapse performance with the collapse performance criteria recommended in SAC/ FEMA guidelines.

The modeling and IDA analyses are done by the use of OpenSEES software published by Pacific Earthquake Engineering Research (PEER) center and by the application of TclEditor computer programming language published by PEER in 2001.

1.3 Organization

Chapter 2 of this research concentrates on a brief literature surveying of the most salient findings in the evaluation of structural collapse including the general methodology for assessing side-sway collapse as well as illustrating the advantages and limitations of the procedure, a brief literature survey on ground motion selection, IDA curves, collapse fragility curves (FCs) and mean annual frequency (MAF) of collapse.

Chapter 3 concentrates on the modeling considerations such as utilized material characteristics, hysteretic behavior of steel01 and steel02 from the manual of OpenSEES software, place of the formation of plastic hinges, an example on the application of P-Δ effect on a cantilever beam modeled by OpenSEES software, explanation about fiber sections, their behavior and the related assumptions, damping in our structures, fatigue phenomena and calibration of Damage Index, DI.

Chapter 4 focuses on the methodology considered in this research for collapse investigations and application in OpenSEES, Ground Motion selection and scaling, post-processing and generating IDA curves and related algorithms used for analyzing SMRFs, discussion of fragility IM-based curve, Log-Normal distribution function and also Fraction-based approach in order to generate fragility curve and finally generating seismic hazard curve in order to find Mean Annual Frequency.

Chapter 5 focuses on analyses and results of two SMRFs according to the methodology discussed in Chapter 4 and representation of the related figures and tables of results.

Chapter 6 of this study is related to the conclusions and discussions as well as recommending possible future works that can be done in this research area.

Chapter 2

LITERATURE SURVEY

2.1 Introduction

“Collapse” in earthquake engineering refers to the incapacity of a structural system or a part of it to maintain gravity load-carrying capacity under seismic excitation that is generally categorized in global and local, respectively [1]. Local collapse may take place, for example, if a column fails in compression or if the shear transfer is lost between a flat slab and a column.

Global collapse has a lot of causes; one of the reasons is the propagation of an initial local failure from element to element that may result in cascading or progressive collapse [2], [3]. The other type of global collapse is “Incremental Collapse” that is because of very large displacement of an individual story and second-order P-Δ effects fully offset the first-order story shear resistance. In both cases, replication of collapse necessitates modeling of deterioration characteristics of structural components subjected to cyclic loading and the consideration of P-Δ effects [1].

In this research, global collapse is expected to be occured due to the incremental “side-sway” collapse of at least one story of the structure by considering deteriorating hysteretic models. This approach permits a redistribution of damage and takes into account the ability of the system to maintain stability until structure P-Δ effects become the deteriorated story shear capacity.

2.2 Previous Research on Global Collapse

Collapse assessment approaches have been improved on several fronts. Understanding and quantifying P-Δ effects and developing deteriorating nonlinear component models that can reproduce experimental results are the intersections of the attempts of researchers up to now [1]. In addition, some studies have been done to integrate all of the factors that influence collapse in a unified methodology. The following is a summary of remarkable studies.

2.2.1 P-Δ Effects

The start point of global collapse is to include the P-Δ effects in seismic response of structures. Although hysteretic models considered a positive post- yielding stiffness, the structure tangent stiffness became negative under large P-Δ effects, on the pattern of leading to collapse of the system [1]. By utilizing springs at the end of the columns of a one-story frame as well as using bilinear hysteretic models, it was concluded that the most significant parameters in collapse are the height of the structure, the ratio of earthquake intensity to the yield level of the structure and the slope of bilinear hysteretic model. Also, they concluded that the intensity of ground motion needed for collapse depends strongly on the duration of ground motion. It is noted that, this was concluded without considering the cyclic behavior [4].

The gravity effect on the dynamic behavior of a SDOF system and its effect on the change of period of the system were also studied and it was shown that the maximum displacement that a system may bear without collapse is directly related to the stability coefficient and the yield displacement of the system [5].

Another study was done in order to consider the previous coefficient in depth and amplification factors were suggested based on the ratio of spectral acceleration generated with and without P-Δ effects. The elastic-plastic SDOF systems and the same stability coefficient for all the period range of interest were considered. Under these assumptions, no significant correlation between amplification factors and natural period was concluded [6]. Some further studies were done to extend the results of previous study to address structures with more complex hysteretic response while considering the P-Δ effect [7].

Two-dimensional moment-resisting frames were analyzed and it was concluded that the minimum strength (base shear capacity) required to withstand a given ground motion without collapse is strongly dependent on the shape of the controlling mechanism. Dynamic instability was evaluated from an equivalent elastic-plastic SDOF system that included P-Δ effects. A remarkable feature of this model is the applicability to buildings that may have different failure mechanisms [8], [9]. The importance of the failure mode had been investigated in a previous research [10], but the former studies had been limited to single-story structures or had been restricted to buildings with global failure mechanisms.

2.2.2 Degrading Hysteretic Models

Bilinear elastic-plastic hysteresis models were firstly used because of their simplicity and then experimental studies illustrate that the hysteretic behavior depends on plenty of structural parameters affect deformation and energy-dissipation characteristics. This dependency was the cause of generating versatile models, such as smooth hysteretic degrading model. This model includes rules for stiffness and strength deterioration but it does not consider a negative stiffness [11].

Another model has the capability of representing cyclic strength and stiffness deterioration based on hysteretic energy-dissipation. This model is a “peak-oriented” that consider pinching based on deterioration parameters. In this model the degradation of the reloading stiffness is based on the maximum displacement that occurred in the direction of the loading path and that’s why it is called a “peak oriented” model. The backbone curve includes a post-capping negative stiffness and residual strength branch. Unloading and accelerated cyclic deterioration are the only models included and before reaching the peak strength the model is incapable of reproducing strength deterioration, because the original backbone curve does not have deterioration [12].

In this study, deteriorating models are developed for bi-linear, peak oriented and pinched hysteretic models vastly discussed in Chapter 3.

2.2.3 Analytical Collapse Investigations

The first attempts to consider P-Δ effects and material deterioration in evaluation of collapse examined the capacity of reinforced concrete frame under seismic excitation. The model was an equivalent SDOF system characterized by degrading tri-linear and quadri-linear (strength-degrading) hysteretic curves [13].

More recently, a systematic study was carried out to assess the effects of prior earthquake damage on peak displacement response of SDOF systems. Prior damage was modeled as a reduction in initial stiffness under neglecting the residual displacements as an assumption; the models were modified to illustrate that SDOF systems with negative post-yield stiffness were prone to collapse whether or not the models had experienced prior damage [14].

The other collapse investigation was done for composite structures consisting of RC columns and steel or composite beams. Second- order inelastic time history analysis were carried out for a given structure and intensity of the ground motion record. The damaged structure was reanalyzed through a second-order inelastic static analysis considering residual displacement and including only gravity loads. When the maximum vertical load the damaged structure could sustain was less than the applied gravity loads, global collapse was assumed to take place otherwise, the record was subsequently scaled up to determine the ground motion intensity at which collapse occurs [15].

Performances of new steel moment-resisting frames were evaluated as a part of FEMA/SAC project. The analytical models included a fracturing element implemented in the Drain-2DX program [16].

IDA concept was employed for estimating the global dynamic instability capacity of a regular RC structure including strength deterioration caused by shear failure of columns [17].

Response of SDOF systems subjected to several ground motion records were studied including P-Δ effects and material deterioration based on Park and Ang damage model [18].

Lateral strengths required to prevent collapse in bilinear SDOF systems with negative post-yielding stiffness was evaluated by detecting a remarkable influence of the period of vibration for short-period systems with small negative post-yield stiffness. Dispersion of the aforementioned lateral strengths and the negative post-

yield stiffness are in the opposite direction, while one increases, the other will decrease [19].

Difference in response of highly nonlinear systems under different analytical formulations was investigated and finally it was concluded that, large displacements formulation produces about the same response as conventional (small displacement) formulations, even in cases that are in vicinity of collapse [20].

2.2.4 Experimental Collapse Investigations

Plenty number of experiments have been carried out to relate collapse with shear failure and finally with axial failure in columns. For example, several reinforced concrete were tested to detect lateral and axial deformation and it was ultimately concluded that the input energy at collapse differ depending on the protocol of loading imposed on each specimen. On the other hand, the vertical and lateral deformations do not vary with the loading path. It was also concluded that collapse takes place when lateral load decreases to 10% of maximum load [21].

Full-scale shear-critical RC building columns under cyclic lateral loads were tested until the column could not sustain the applied axial load. The tests showed that the loss of axial load capacity does not follow immediately after loss of lateral load capacity, necessarily [22].

Other study concluded that shear failure in columns does not necessarily lead to collapse of the system. Several factors affect reduction of axial load capacity that shear failure is usually accompanied by that. It was obtained that in columns having lower axial loads, failure takes place at relatively large drifts, without considering either shear failure had just taken place or shear failure had taken place at much

smaller drift ratios. For columns with larger axial loads, failure due to axial load will occur at smaller drift ratios and might occur almost immediately after loss of lateral load capacity. This research was also collected data for developing an empirical model to estimate shear strength deterioration [23].

A series of shaking table tests of a SDOF steel frame systems were done subjected to earthquakes of progressively increasing intensity up to collapse due to P-Δ effects (geometric nonlinearity) and it was concluded that stability coefficient has the most important effect on the structural behavior. There was a decrease in the maximum sustainable drift and spectral acceleration that could be resisted before collapse while this coefficient increases [24]. In order to extend the previous work, testing additional SDOF systems was done and it was detected that current methods of nonlinear dynamic analysis as the OpenSEES platform are very accurate for estimating collapse for systems that the P-Δ effect dominates the onset of collapse [25].

In conclusion, although the plenty numbers of research have been done on this topic, the response of structures has not been investigated in detail under the combination of geometric nonlinearities and material deterioration for Steel Moment Resisting Frames. Therefore, a need exists to carry out systematic research on global collapse considering all sources lead to this limit state.

2.3 Incremental Dynamic Analysis

Fortunately, improvements in computer processing power and developed software engineering make it possible to move toward an increasingly accurate but coincidentally more complex analysis methods. The old concept of scaling ground

motion records (scaling to the design spectrum) and conventional nonlinear dynamic analysis was about running one to several different records, each one, to produce one to several “single-point” analyses mostly used for checking the designed structures. On the other hand, nonlinear static analysis methods in a “continuous” picture investigate the complete range of structural behavior and facilitate our understanding. By analogy with passing from a single static analysis to the incremental static pushover, an extension of a single time-history analysis to an incremental one where the seismic loading is scaled establishes the current state of the art. This concept was mentioned by many researchers since 1977 (by Bertero) in research literatures in several forms. A few years ago, United States Federal Emergency Management Agency (FEMA) guidelines adopted this concept as Incremental Dynamic Analysis (IDA) to determine global collapse capacity. Now, IDA is widely applicable method and multi-purpose study and it can provide accurate estimation of the complete range of the model response. IDA objectives are summarized below [26]:

- How the structure behaves in a rare and stronger ground motion level.
- Estimating the dynamic capacity of the global structural system.
- Producing a complete picture of the range of the demand versus the range of the potential levels of earthquake ground motion record.
- How the nature of the structural response changes as the intensity of earthquake ground motion increases.
- Putting all above concerns in a multi-record IDA study to investigate how stable or variable are these from one earthquake ground motion record to another.

As it was explained before, IDA method basically takes the old concept of scaling ground motion records and develops it into a way to accurately describe the full range of structural behavior to collapse. In this method a structural system is subjected to ground motion records scaled to multiple levels of intensity. This will yield response curves, parameterized versus intensity level. Finally, by defining the limit-state and combining the results with standard Probabilistic Seismic Hazard Analysis (PSHA), one can reach the aims of performance-based earthquake engineering [27].

2.4 Selection of Ground Motions

The approach of collapse is based on time history analysis. Therefore, a set of ground motions must be carefully selected according to specific objectives. The GM set should be large enough to provide reliable statistical results. For mid-rise buildings, ten to twenty ground motions records are usually enough to provide sufficient accuracy to estimate behavior of structure under seismic loads and its seismic demand [28]. The more ground motion records undoubtedly result more accurate response of structures in order to decrease record to record uncertainty (RTR) and hopefully by the use of powerful computers and using OpenSEES Software it is possible to perform analyses for forty four ground motion records as discussed in Chapter 4.

2.5 Collapse Fragility Curves and Mean Annual Frequency of Collapse

Computation of the mean annual frequency (MAF) of collapse is a direct application of collapse capacity evaluation. MAF of collapse is developed from collapse capacities for a set of ground motions and it is assumed that the distribution is lognormal and the first and second order moments are computed from individual

point of collapse. This information is utilized to generate the cumulative distribution function (CDF) corresponds to a fragility curve and describes the probability of collapse that may be very sensitive to the hysteretic properties of the system. For computing the mean annual frequency of exceeding, the fragility curves should be normalized by a specific standard deviation value that defines the strength of the structural system [1]. Once a fragility curve is computed and hazard information for the site is available, the mean annual frequency of collapse can be computed as follows [29]:

(2.1)

Where:

$F_{C,Sa,c}(x)$: Probability of S_a capacity

$S_{a,c}$: Exceeding x

$\lambda_{Sa}(x)$: Mean annual frequency of S_a exceeding x (ground motion hazard)

$F_{C,Sa,c}(x)$ corresponds to the fragility curve obtained from individual collapse capacities.

2.5.1 Collapse Fragility Curves (FCs)

A fragility function for a limit state represents the conditional probability of exceeding the limit state capacity for a given level of ground motion intensity. The aim is to estimate the limit state of collapse by utilizing the spectral acceleration at the fundamental period of the system as the ground motion is intensified. Therefore, the FC for these conditions is:

(2.2)

Where:

$F_{C,\,Sa,c}(x)$ Corresponds to the value of the fragility curve (FC) at spectral acceleration, x, for the limit state of collapse, i.e., the "Collapse fragility curve". By considering that the demand ($S_a = x$) is statistically independent of the capacity of the system ($S_{a,c}$), the FC is expressed as the probability of being S_a less than or equal to x. The collapse FC is shown also as a cumulative distribution function (CDF) of random variable, the collapse capacity, $S_{a,c}$.

In literatures, "Collapse Capacity" is used as the parameter for collapse evaluation. This parameter is normalized and defined as the ratio of ground motion intensity to a structural strength parameter when collapse takes place. Thus, it is possible to generate "normalized collapse fragility curves" instead of the ground motion intensity. One of the advantages to assess collapse according to the relative intensity (collapse capacity) is that the parameter is easily de-normalized and plugged in Equation 2.2 directly [1].

2.5.2 Mean Annual Frequency of Global Collapse (MAF)

The mean annual frequency of collapse (λ_c) is obtained when the normalized fragility curves of the system and hazard curves for the site of interest are available. The MAF of collapse is defined as the mean annual frequency of strong motion intensity (S_a) becomes larger than collapse capacity multiplied by the probability of having such a strong motion intensity:

(2.3)

Where:

$f_{Sa}(x)$: The probability density function (PDF) at the spectral acceleration value x given an event of interest.

v: The annual rate of occurrence of such events (rate of seismicity).

As it is known, the first term of the integral was defined as the collapse fragility curve. Thus:

(2.4)

The PDF of the spectral acceleration value is defined as the complementary cumulative distribution function (CCDF) [17]:

(2.5)

Where:

$CCDF[G_{Sa}(x)]$: The probability of exceeding a certain value

$CDF[F_{Sa}(x) = f_{Sa}(x).dx]$; The probability of being less than or equal to a certain threshold.

Thus, their derivatives are equal in absolute values but have opposite signs. By substituting Equation 2.5 in Equation 2.4:

(2.6)

Also:

(2.7)

Where:

$D\lambda_{Sa}(x)$: The spectral acceleration hazard. So:

(2.8)

The MAF of collapse in terms of the collapse fragility curve for a given median base shear strength over a S_a hazard curve pertaining to a specific site is explicitly expressed by Equation 2.8.

Note that this approach called “IM-Based approach” is more straightforward than the other methodology for calculating collapse based on displacement demands and capacities. The “EDP-Based approach” breaks down the collapse limit state into two steps and requires an additional integration [17]. First, the EDP hazard is calculated as the probability of exceeding a demand threshold given that the IM is equal to a certain value; x. In a second step, the probability of collapse is calculated as the probability of having an EDP demand hazard larger than the EDP capacity. Therefore, evaluation of global collapse based on the relative intensity of the system facilitates the calculation of the mean annual frequency of collapse [1].

Chapter 3

MODELING

3.1 Introduction

The results of a nonlinear analysis are mainly based on the modeling assumptions. At least some basic principles are significant in modeling:

- Material behavior
- Damping
- Modeling of elements behaviors
- Considering or neglecting of the large deformations and large stresses
- Step by step analysis algorithm under earthquake loads
- Analysis algorithm of each step

In modeling for the aim of nonlinear analysis, according to the type of analysis, the behavior of materials should be considered in suitable forms. For example, in order to analyze under cyclic loads, the cyclic behavior of the materials should be clearly understood and a consistent mathematical models should be utilized. In contrast, when the aim is static analyses and in obvious word nonlinear static analyses, loading has just one direction so, the mathematical behavior of the material is different. Also, if this type of analyzing is substituted by dynamic analysis, appropriate assumptions should be contrived [30], [31].

In this chapter, after a short review on hysteretic behavior of steel, the accuracy of considered models will be improved by introducing the mathematical modeling provided in OpenSEES software, defining the parameters of these models and determining or defining the appropriate values of those parameters. In general, some concepts are mentioned:

- Steel behavior in elastic zone
- Steel behavior after yielding
- Changing of the behavior of steel due to cyclic loading
- Cyclic strength degradation

The last one usually occurs because of starting or propagating the micro-cracks [30].

3.2 Plastic Cycles of Steel

By increasing the domain of loading or by increasing the number of cycles in cyclic loading, the structural steel becomes harder and in other words, it can experience the larger stress-strain cycles. Figure 3.1 shows an example of stress-strain cycle of a structural steel that is made of steel of type A-36. In current example, the hardening is more than 40% [31].

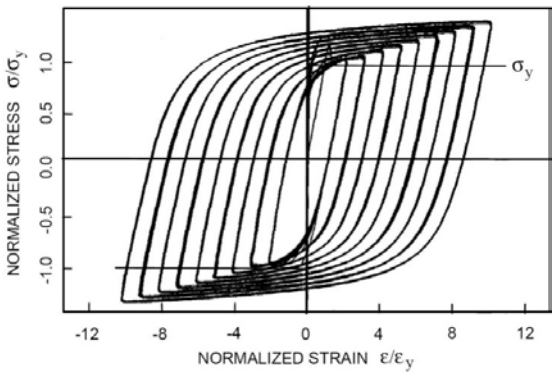

Figure 3.1: Cyclic Stress-strain diagram of structural steel of Type A-36

Starting and propagating cracks will be problematic when the strain domain or number of cycles is very large and this will ultimately results the stress degradation in cycles and finally it will be the cause of failure. Therefore, steel looks a suitable material for the structures that should dissipate energy due to nonlinear behavior [31].

In parallel with the suitable cyclic behavior, there are some probable weaknesses. The first weakness is due to tensile loading. Local defect, even small, may result very large stresses and finally can be the cause of the formation of cracks and failure. Particularly if that crack is in the direction of thickness of steel element (for example, thickness of steel plates). Such defect may occur in production phase, assembling the elements and structural parts. Shortly, it has lots of sources but, the most important cause is due to welding problems at the intersection of base metal and welding metal. Crack formations and propagations may start at the points of stress concentration such as coped parts, wall of bolt holes or chopped edges of steel plates. Therefore, there are limitations in codes and standards for methods of punching and plate chopping particularly in higher thicknesses. For example, drilling is better than

punching in order to make holes for thick plates, although punching is more economical and has a better final appearance [31].

Propagation and enlargement of cracks to the critical values will be the cause of instantaneous failure and unexpected decrease of strength, like what is shown in Figure 3.2. This figure is related to the response of force- displacement of a cantilever beam made of steel. Instantaneous decrease in strength is because of weld failure of the connection of the upper flange of beam [31].

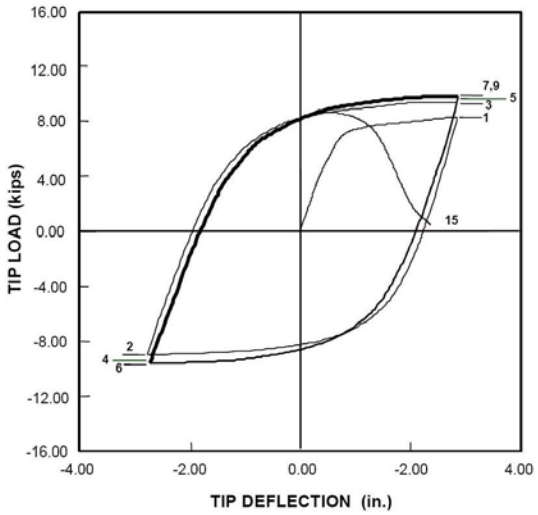

Figure 3.2: Load- deformation response showing rapid deterioration

The second problem is related to the compressive loading. One steel section is generally consisted of steel plates manufactured by different methods such as warm and cold forming, total or staggered welding due to the length of element. Each plate, individually, has the capacity of local buckling and after local buckling occurs in section compnents, gradual decrease in strength and stiffness of element will take place, like what is demonstrated in Figure 3.3. The most significant factors affect on elemental buckling and also the behavior of the structural elements after buckling are connection conditions and slendernness ratio (width over thickness of section). Most

of manuals and handbooks recommend criteria of controlling premature buckling of components of the sections and they are usually based on limiting the slenderness ratio. The aim of such a criterion is “the inclinity” to pospone the local buckling to the large magnnitudes of strain, that in expected strains during high intensity earthquakes, these strains will not result inappropriate strength [31].

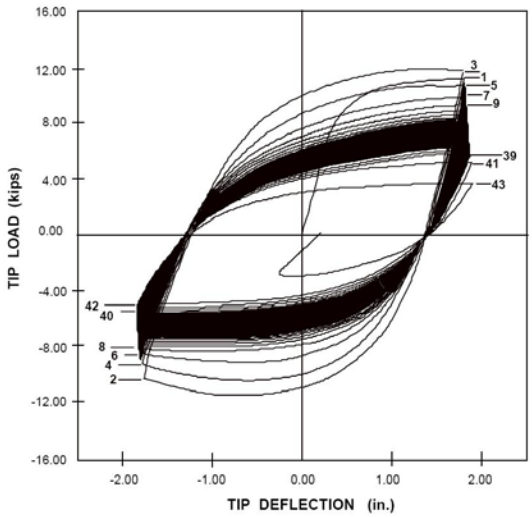

Figure 3.3: Load-deformation response showing gradual deterioration

The other phenomenon decreases the strength and stiffness of elements is lateral torsional buckling (LTB). This phenomenon is related to the bending elements and mainly, I-shape beams those torsional capacities are very low and shortly, take place when the element is loaded on the strong axis, the torsional stiffness is low and the strong axis is very stronger than the weak axis. In these conditions, the element would rather to have sidesway than to bend. The cause of this event is the buckling tendency of compressive web and resistance of tensile web to the sidesway, simultaneously. Among all of the effective factors, unbraced length and bending moment variations are more remarkable. If the unbraced length of compressive web is controlled, this phenomenon will be limited. Also, I-shape sections can be replaced by H-shapes (wide flanges) that because of the nearer stiffness values of two axes

will be better in behavior (variations of moment of inertia of weak axis for I and H sections with respect to the width of the web is third order and for the strong axis it is first order). Because of this phenomenon, a similar figure like Figure 3.3 is obtained but just the trend of stiffness decrease will be greater [31].

Two major investigations followed in cyclic behavior of steel are; Bauschinger effect [32] and Isotropic hardening [33]. Figure 3.4.a shows the stress-strain diagram under incremental static loading. In this figure, two remarkable characteristics of steel in plastic zone is visible, one in the identified yielding point and the other is plastic zone and strain hardening after that.

According to Figure 3.4.b, if the loading direction changes to the opposite direction at point A, the stress-strain curve descends with the equal slope of elastic part. After tensile stress vanishes, not any specified yielding point is recognized in compression. So, the identified yielding point of steel occurs at the half-cycle of the first nonlinear cycle (without mentioning whether this half-cycle is due to tensile or compressive loading). Promptly started the inelastic behavior in cyclic behavior of steel is called Bauschinger effect [32], [33].

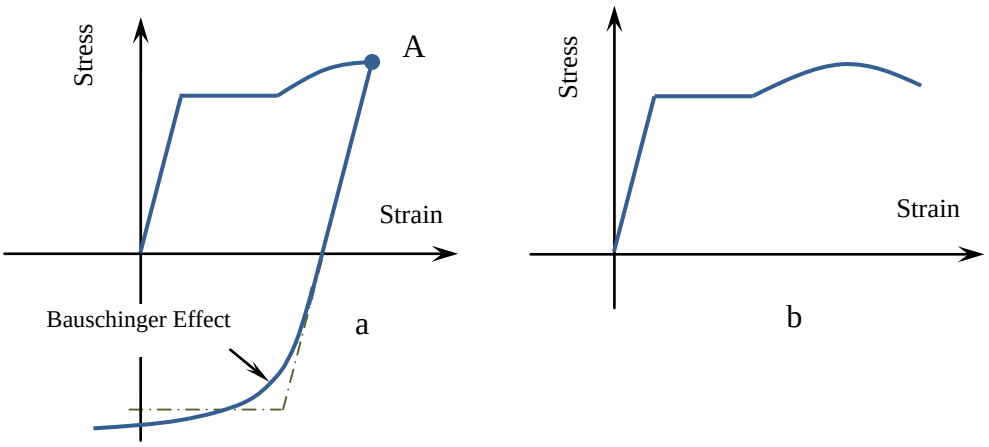

Figure 3.4: Stress-strain diagram of structural steel. (a) Stress-strain diagram of structural steel for cyclic loading. (b) Stress-strain diagram of structural steel under incremental static loading.

Figure 3.5 illustrates the stress- strain diagram of a sample that its strain of unloading is less than the strain of starting strain hardening. In this condition, beside Bauschinger effect, steel will move horizontally on the yielding line known as plastic zone. In first cycle that loading enters strain hardening; the horizontal line is not visible. After passing yielding point in each cycle, strain hardening is started. In other words, horizontal line and hardening after that is visible just once (the same as identified yielding point explained in Figure 3.4.) [32].

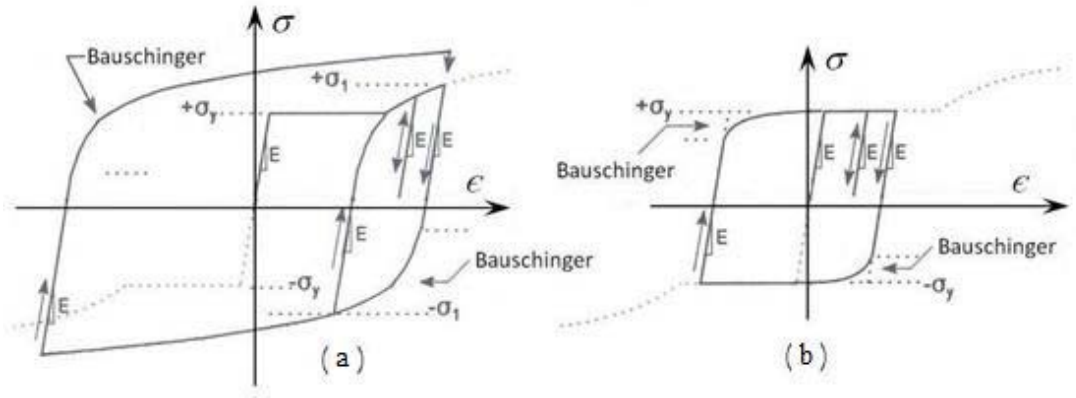

Figure 3.5: Cyclic stress-strain diagram of structural steel. (a) With strain hardening. (b) Without strain hardening.

3.3 Menegotto-Pinto Model

This model is initially suggested by Giuffré and Pinto. After that, Menegotto and Pinto improved that model and published in 1973 [32]. The material recommended in OpenSEES named Steel02, is the result of corrections and improvements of Filippou and his group on the parameters of hardening that was published in 1983 in System International units (Figure 3.6.).

Steel02 is capable to consider the Bauschinger effect as well as strain hardening in nonlinear cycles.

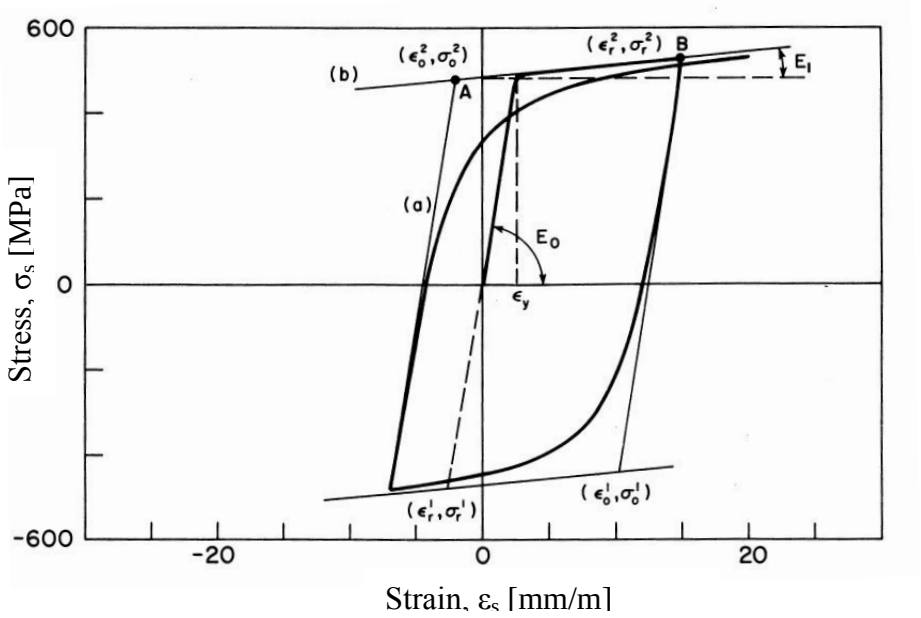

Figure 3.6: Menegotto- Pinto model of steel.

Equation 3.1 shows the manner of passing the tangent line with slope of E_0 to the other tangent with slope of E_1 (lines a and b in Figure 3.6).

(3.1)

(3.2)

(3.3)

Where:

σ_0 and ε_0: Stress and strain at the intersection of the tangents (point a at Figure 3.6).

σ_1 and ε_1: Stress and strain at the point where unloading is started.

b: Hardening ratio; E_0 / E_1.

R: A parameter that identifies the transient curve between two tangents (lines a and b in Figure 3.6). This parameter is identified by ζ, strain difference between intersection of two tangent lines of the last cycle (point A in Figure 3.7) and corresponding strain of the unloading point of prior cycle (point B in Figure 3.7). The related equation of R is as follow:

(3.4)

Where: the values of R_0, a_1 and a_2 are determined experimentally. R_0 is the value of R at the first half-cycle (Figure 3.7)

If the data of prior cycles are available and unloading takes place, the reloading path will be in the direction of the previous path so, it is needed to keep all of the required information to check all of the incomplete cycles in order to continue loading (part a of Figure 3.8). Keeping all of such this information is not possible. Therefore, data related to a limited number of pre-identified cycles are kept. In Menegotto-Pinto model, this information is as follow:

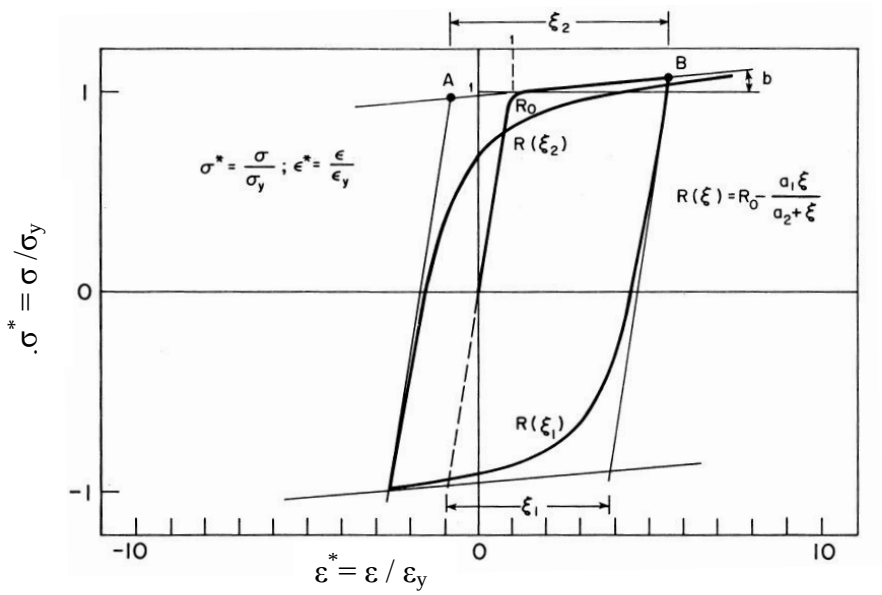

Figure 3.7: Definition of *R(ζ)*, curvature parameter in Steel02, for plastic cyclic behavior

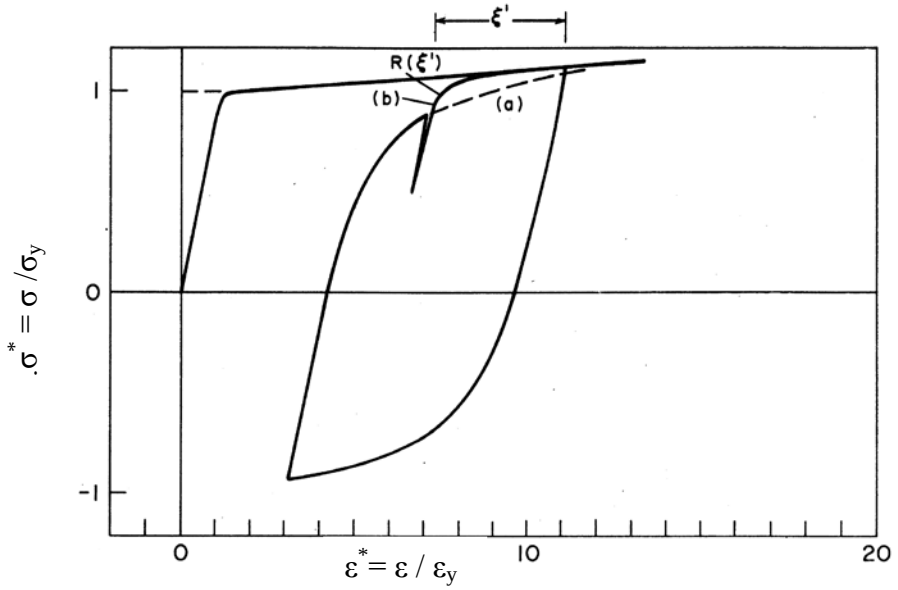

Figure 3.8: Definition of *R(ζ),* curvature parameter in Steel02, for incomplete plastic cycles

According to the above limitations, for continuing an incomplete cycle in reloading, instead of continuing in direction of curve a (Figure 3.8) it will follow the path of curve b. However, this difference between the recommended models and actual models can be neglected.

Recommended models consider the effects of hardening by means of transferring the tangent of plastic zone before determining the intersection point of new cycle. Value of plastic tangent displacement is shown by σ_{st}. This is firstly suggested by Stanton and Mc Niven that they intended to move both of stress and strain on the stress-strain envelope curve.

— —— (3.5)

Where: ε_{max} is the absolute value of unloading strain, σ_y and ε_y are yielding stress and yielding strain respectively and a_3 and a_4 are identified by the experiment. a_3 stress displacement and a_4 is the strain displacement.

Therefore, eight parameters are needed to identify a sample of steel perfectly by Menegotto-Pinto modeling method:

- E_0: Slope of elastic zone.
- E_1: Slope of plastic zone (its ratio to the slope of elastic zone line, b).
- σ_y: Yielding stress.
- R_0: Radius of transient zone in half- cycle of the first cycle.
- a_1 and a_2: Parameters of curvatures of transient zones in cycles.
- a_3 and a_4: Strain hardening parameters.

Menegotto-Pinto is nominated as Steel02 command in OpenSEES and it is identified in the section 3.4.

3.4 Steel01 Material Modeling in OpenSEES Software

The Steel01 command is used to construct a uniaxial bilinear steel material object with kinematic hardening and optional isotropic hardening described by non-linear evolution equation [34].

UniaxialMaterial Steel01 $matTag $Fy $E0 $b <$a1 $a2 $a3 $a4>

$matTag: Unique material object integer tag

$Fy: Yield strength

$E0: Initial elastic tangent

$b: Strain-hardening ratio (ratio between post-yield tangent and initial elastic tangent)

$a1, $a2, $a3, $a4: Isotropic hardening parameters: (optional, default: no isotropic hardening)

$a1: Isotropic hardening parameter, increase of compression yield envelope as proportion of yield strength after a plastic strain of *$a2*($Fy/E0)*

$a2: Isotropic hardening parameter (see explanation under *$a1*)

$a3: Isotropic hardening parameter, increase of tension yield envelope as proportion of yield strength after a plastic strain of *$a4*($Fy/E0)*

$a4: Isotropic hardening parameter (see explanation under *$a3*)

Figure 3.9 to 3.12 illustrate the static and dynamic (hysteretic) behavior of Steel01 material in tension and compression.

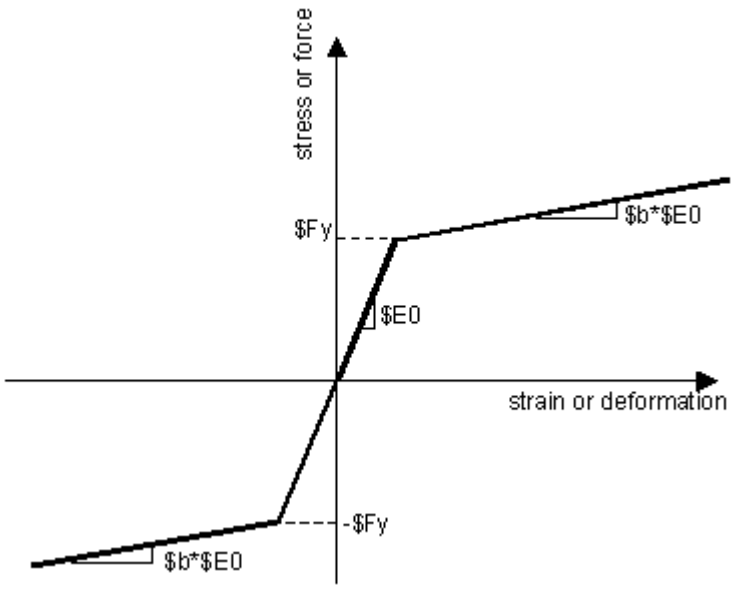

Figure 3.9: Steel01 Material, Material Parameters of Monotonic Envelope

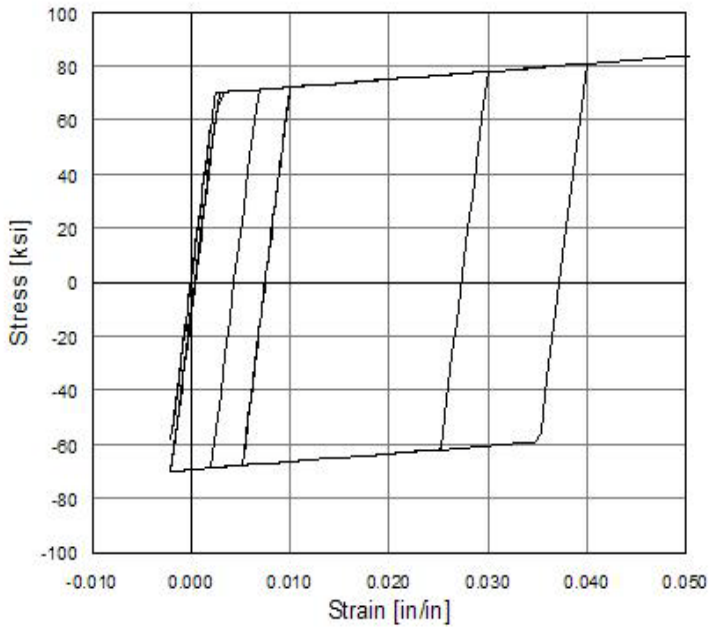

Figure 3.10: Steel01 Material, Hysteretic Behavior of Isotropic Hardening Model

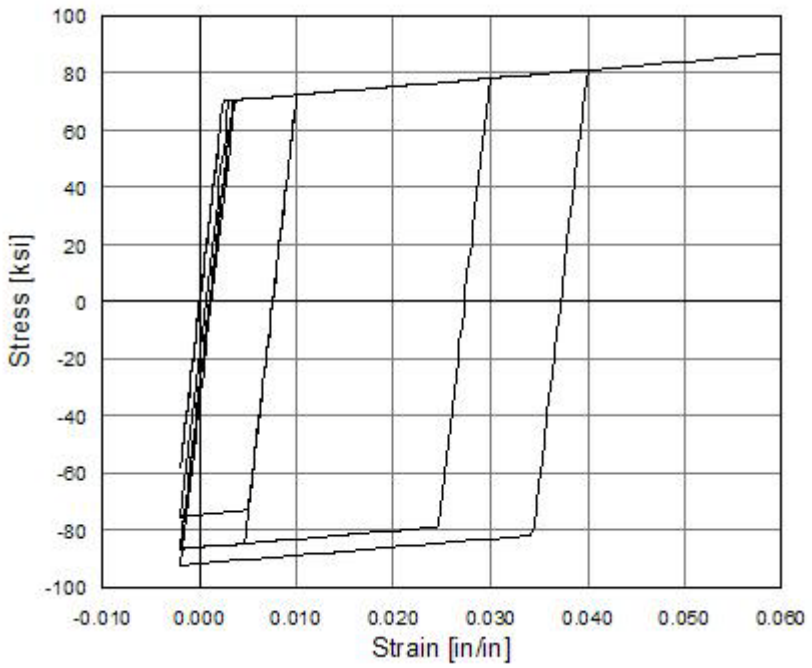

Figure 3.11: Steel01 Material, Hysteretic Behavior of Model with Isotropic Hardening in Compression

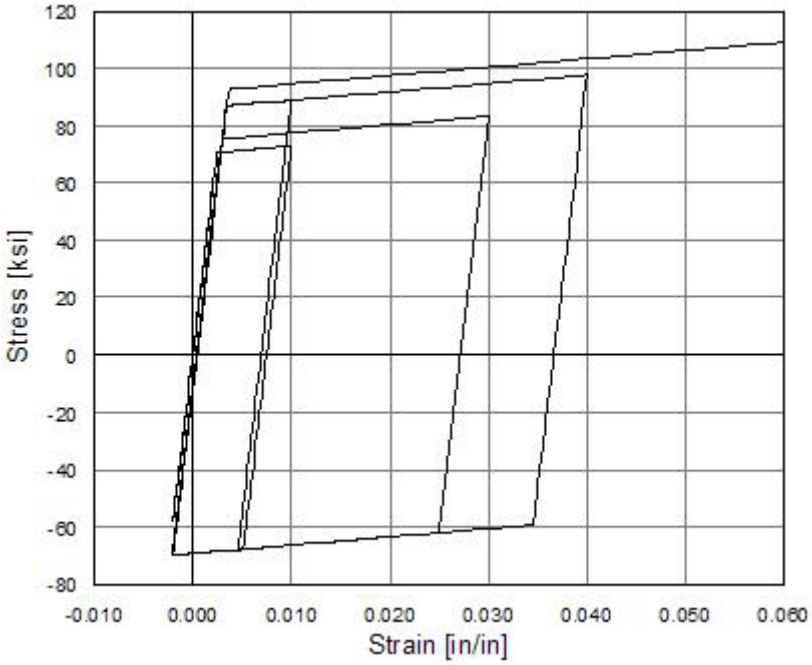

Figure 3.12: Steel01 Material, Hysteretic Behavior of Steel01 Model with Isotropic Hardening in Tension

3.5 Steel02 Material Modeling in OpenSEES Software; Giuffré-Menegotto-Pinto Model with Isotropic Strain Hardening

The Steel02 command is used to construct a uniaxial Giuffre-Menegotto-Pinto steel material object with isotropic strain hardening [35].

uniaxialMaterial Steel02 $matTag $Fy $E $b $R0 $cR1 $cR2 <$a1 $a2 $a3 $a4 $sigInit>

$matTag: Unique material object integer tag

$Fy: Yield strength

$E: Initial elastic tangent

$b: Strain-hardening ratio (ratio between post-yield tangent and initial elastic tangent)

$R0, $cR1, $cR2: Control the transition from elastic to plastic branches. Recommended values: *$R0*=between 10 and 20, *$cR1*=0.925, *$cR2*=0.15

$a1, $a2, $a3, $a4: Isotropic hardening parameters: (optional, default: no isotropic hardening). Default values for no isotropic hardening: *a1* = 0.0; *a2* = 1.0; *a3* = 0.0; *a4* = 1.0

$a1: Isotropic hardening parameter, increase of compression yield envelope as proportion of yield strength after a plastic strain of *$a2*($Fy/$E)*

$a2: Isotropic hardening parameter (see explanation under *$a1*)

$a3: Isotropic hardening parameter, increase of tension yield envelope as proportion of yield strength after a plastic strain of *$a4*($Fy/$E)*

$a4: Isotropic hardening parameter (see explanation under *$a3*),

$sigInit: Initial Stress Value (optional, default: 0.0), the strain is calculated from *epsP=$sigInit/$E*, if (*sigInit!= 0.0*) { double *epsInit = sigInit/E: eps = trialStrain+epsInit: }* else *eps = trialStrain* [35].

Figure 3.13 to 3.16 illustrate the static and dynamic (hysteretic) behavior of Steel01 material in tension and compression.

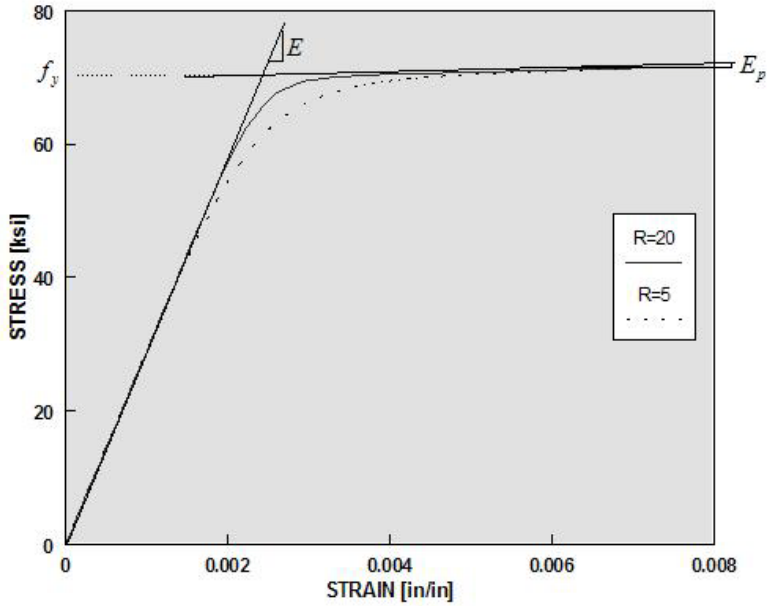

Figure 3.13: Steel02 Material, Material Parameters of Monotonic Envelope

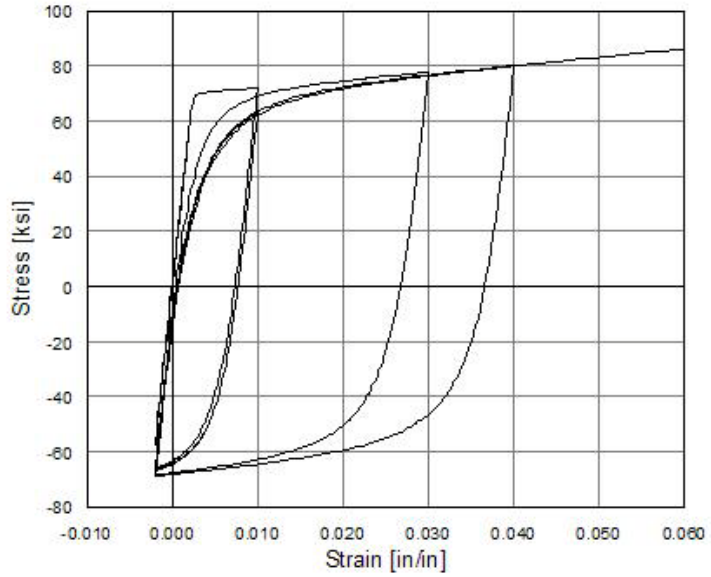

Figure 3.14: Steel02 Material, Hysteretic Behavior of Steel02 Model with Isotropic Hardening in Tension

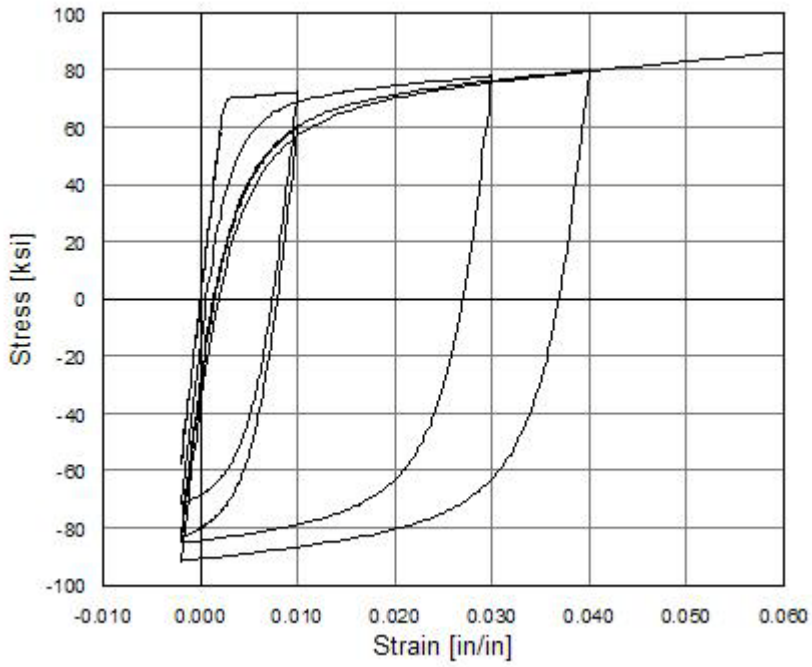

Figure3.15: Steel02 Material, Hysteretic Behavior of Model with Isotropic Hardening in Compression

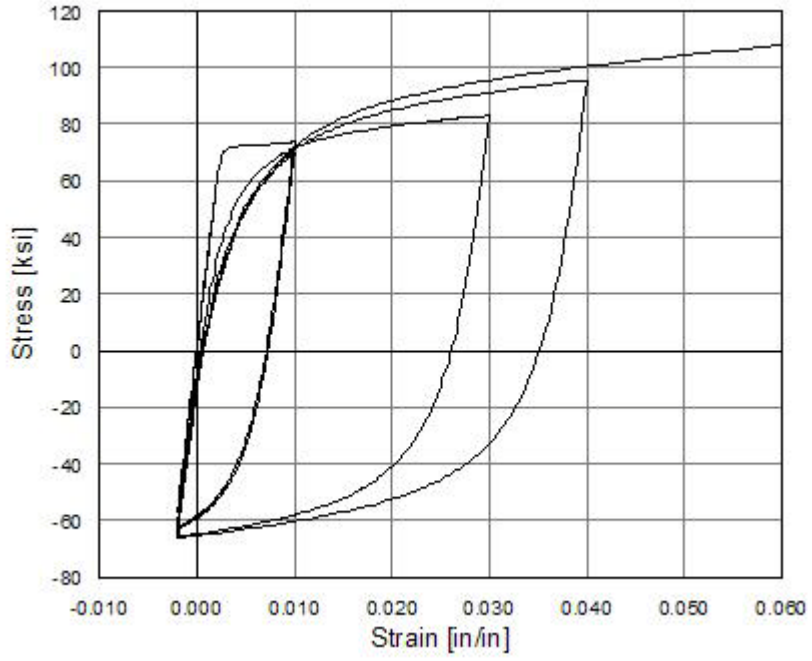

Figure3.16: Steel02 Material, Hysteretic Behavior of Model with Isotropic Hardening in Tension

3.5 Frames Characteristics and Investigations

Frames used here, are 3 and 9 story SAC/FEMA steel project pre-Northridge designed structures, located at Los Angeles, California on soil type II, and were designed to conform *h/400* as inter story lateral drift ratio requirement. Figure 3.17 shows plan of buildings [31].

An “archetype” (in terminology of ATC-63 project) 2-D modeling is presented here and consists of one of North-South perimeter moment resisting frame from each building. Cross sectional and material properties of frames are shown in Tables 3.1, 3.2 and 3.3, respectively [31]. Table 3.4 and 3.5 describes values of dead load and live load in nonlinear analysis and total mass at each floor, intended to model induced lateral earthquake load, respectively. This total floor mass must distribute to the main nodes at each story, excluding dummy column nodes.

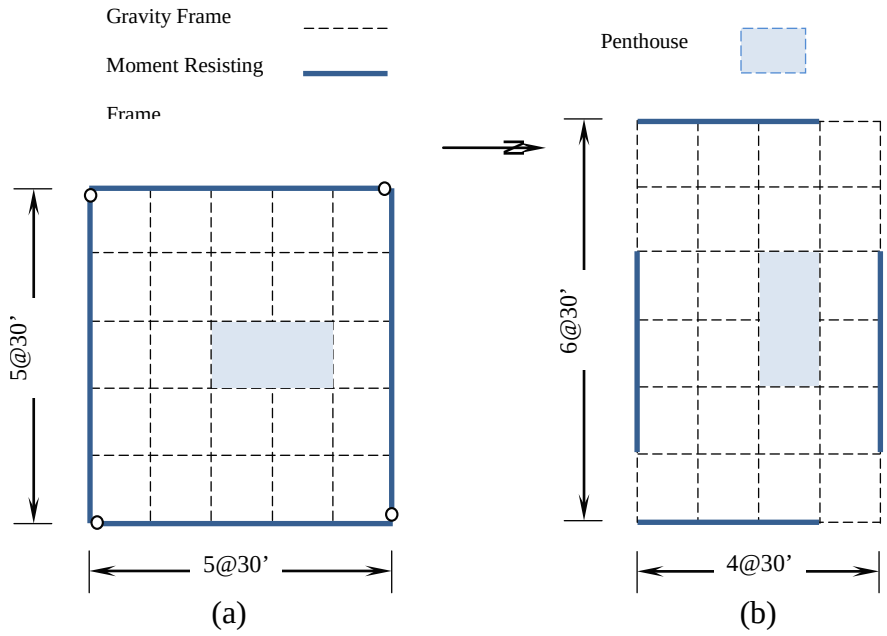

Figure 3.17: Plan of 3 and 9 story frames and location of gravity and moment resisting parts. (a) Nine story frame, (b) three story frame.

Table 3.1: Overview of beam and column sections of 3 - story frame

3 - story frame						
floor/floor	Rigid Frame			Gravity Frame		
	Columns		Beams	Columns		Beams
	Exterior	Interior		under penthouse	others	
1/2	W14x257	W14x311	W33x118	W14x82	W14x68	W18x35
2/3	W14x257	W14x311	W30x116	W14x82	W14x68	W18x35
3/Roof	W14x257	W14x311	W24x68	W14x82	W14x68	W16x26

Table 3.2: Overview of beam and column sections of 9- story frame

9 - story frame						
floor/floor	Rigid Frame			Gravity Frame		
	Columns		Beams	Columns		Beams
	Exterior	Interior		under penthouse	others	
-1/1	W14x370	W14x500	W36x160	W14x211	W14x193	W21x44
1/2	W14x370	W14x500	W36x160	W14x211	W14x193	W18x35
2/3	W14x370 W14x370	W14x500 W14x455	W36x160	W14x211 W14x159	W14x193 W14x145	W18x35
3/4	W14x370	W14x455	W36x135	W14x159	W14x145	W18x35
4/5	W14x370 W14x283	W14x455 W14x370	W36x135	W14x159 W14x120	W14x145 W14x109	W18x35
5/6	W14x283	W14x370	W36x135	W14x120	W14x109	W18x35
6/7	W14x283 W14x257	W14x370 W14x283	W36x135	W14x120 W14x90	W14x109 W14x82	W18x35
7/8	W14x257	W14x283	W30x99	W14x90	W14x82	W18x35
8/9	W14x257 W14x233	W14x283 W14x257	W27x84	W14x90 W14x61	W14x82 W14x48	W18x35
9/roof	W14x233	W14x257	W24x68	W14x61	W14x48	W16x26

Table 3.3: Mechanical Properties of steel material used [37]

Section	Steel Material	F_y (ksi)	F_u (ksi)	R_y	R_t	E (ksi)
Beams	A36	36	58	1.5	1.2	29000
Columns	A572-Grade 50	50	65	1.1	1.1	

Table 3.4: Values of dead and live load used in nonlinear analysis

Floor Dead Load (including 13psf as steel weight)	96 psf
Roof Dead Load (excluding penthouse)	83 psf
Penthouse	116 psf
Reduced Live Load (Floors and Roof)	20 psf

Table 3.5: Values of total floor mass used in the model for calculation of induced floor horizontal load due to earthquake

3-Story Frame	**m** (kips-sec^2/ft)
Roof	70.90
2nd / 3rd Floor	65.53

9-Story Frame	**m** (kips-sec^2/ft)
Roof	73.10
3rd – 9th Floor	67.86
2nd Floor	69.04

A dummy column is modeled to account for P-Delta effect on seismic response of system, representing effect of gravity load on gravity columns which are eliminated in 2-D modeling. The dummy column will then be under action of half of total gravity load of each floor. Table 3.6 illustrates vertical load to be applied on dummy column at each level. Properties of dummy column section are based on fifty percent of all gravity columns as well as contribution of East-West perimeter moment resisting frame columns (see Figure 3.23).

Table 3.6: Values of floor load to be applied on the dummy column

3-Story Frame	**Total Load** (kips)	**50%** (kips)
Roof	2284.2	1142.1
Floors	2505.6	1252.8

9-Story Frame	**Total Load** (kips)	**50%** (kips)
Roof	2376.9	1188.45
Floors	2610	1305

Except for dummy columns, all beams and columns are modeled using "nonlinearBeamColumn" element in OpenSEES [34], a forced based inelastic element which accounts for the distributed inelasticity through integration of material response over the cross section, defined as a fiber section and subsequent integration of section response along the element. Its drawback is to following Bernoulli principle which assumes that plain section remains plain, so distribution of strain in the depth of cross section is linear even in high levels of inelasticity and subsequently does not account for local buckling and its effects on decreasing the fatigue life of structural steel elements at the location of plastic hinges.

Steel material used here is bilinear model with positive post elastic slope of 0.003 times the initial elastic slope of steel (i.e. modulus of elasticity equals to 29000 ksi), representing strain hardening. This model is named as "Steel01" in OpenSEES [34] a schematic of stress-strain curve of material model used is shown in Figure 3.18. Although this model can consider isotropic hardening, to account for shift of yield envelop in cyclic response, our modeling excludes this phenomenon. Also steel01 does not model Bauschinger [36] effect. As discussed, value 29000 ksi is used as modulus of elasticity. Yield stress of steel material in modeling of beams and columns both, is modified by implementing R_y, a value recommended by seismic provisions of AISC [37], to account for randomness in material properties, especially the yield stress. So instead of F_y, values of R_yF_y equals to 54 ksi and 55 ksi are used in modeling of beams and columns respectively (See Table 3.3).

To account for large displacement, we can use "P-Delta" or a more precise model, "co rotational" geo-transformer in OpenSEES [34]. The later is proposed by Remo M. de Souza, which can be found in more detail in literature [38]. In general,

OpenSEES considers geometric nonlinearities by means of incorporating different types of geometric transformation which are aimed to transform stiffness matrix of each element from its basic (local) coordinate to general (global) one. Taking in to account large deformations, which may be termed the second order analysis, is important for those elements supporting axial load, such as dummy column we have defined. Figure 3.19 illustrates this concept more. A cantilever column (Figure 3.20) supporting axial load of P, is to be analyzed under the action of lateral load of F_{EQ} equal to V_b. Eliminating application of gravity loads on lateral displacement, i.e. P-Delta effect, causes moment equilibrium equation similar to Equation (3.6), while considering it, results in Equation (3.7), obviously made the overturning moment to increase due to P-Delta. In contrast, consideration of P-Delta effects decrease base shear as shown in Figure 3.21. So for beams and columns of main frame, it is not necessary to use second order analysis and using “Linear” geo-transformer seems to be sufficient, but for dummy column other types of geometric transformation should be used.

— (3.6)

— — (3.7)

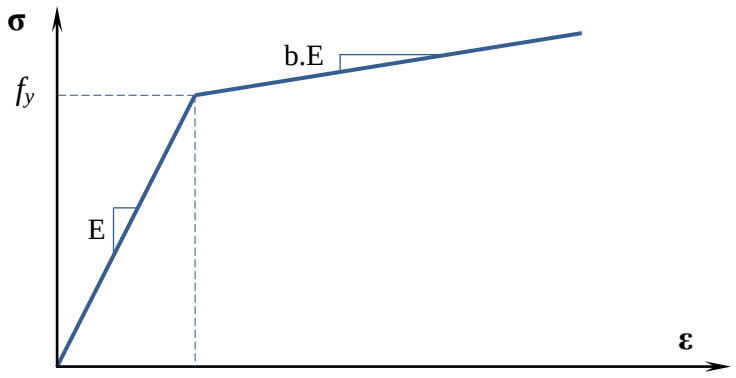

Figure 3.18: A schematic of stress-strain curve of material model

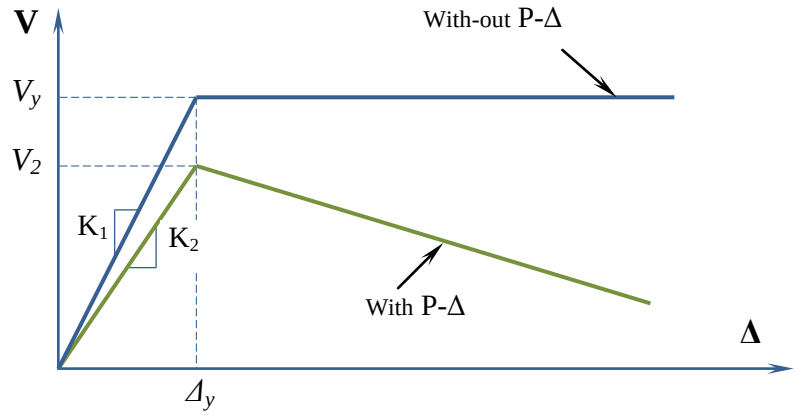

Figure3.19: Second order analysis by means of considering P- Δ effects

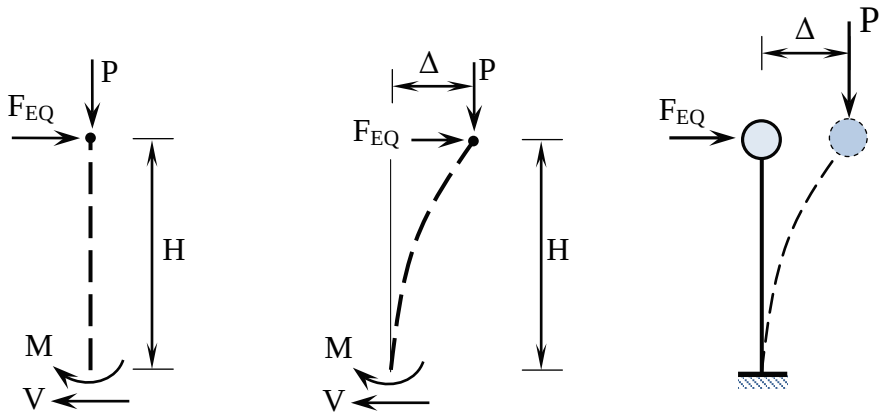

Figure 3.20: A cantilever column supporting axial load of *P*, is to be analyzed under the action of lateral load of F_{EQ} equal to V_b

Example: To briefly describe the type of geometric transformation that should be used for dummy column, a W12x106 cantilever column is modeled under the action of axial load equals $0.2P_{cr}$. The column is then pushed monotonically until its top displacement reaches 4 inches. Using different types of geometric transformation, capacity curve of column is shown in Figure 3.21. As illustrated in this figure, generally there is no difference between "P-Delta" and "co-rotational" geo-transformation in OpenSEES for modeling P-Delta effect in dummy column.

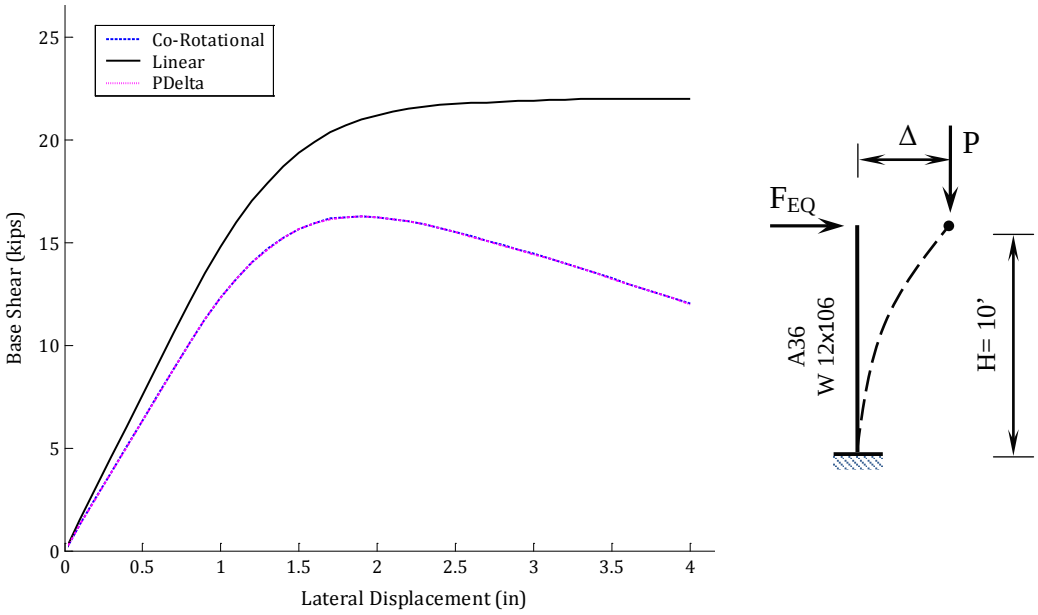

Figure 3.21: Consideration of P-Delta effects decrease base shear

Modeling of damping for dynamic analysis is based on Rayleigh damping [39]. It assumes that the damping matrix *C* is proportional to stiffness, *K*, and mass, *M*, matrixes.

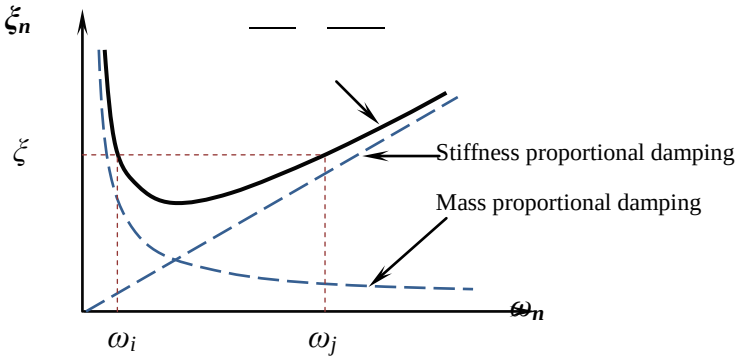

Figure 3.22: Variation of modal damping ratio with natural frequency in Rayleigh damping

Assuming mass and stiffness proportional (Rayleigh) damping, we have

(3.8)

Pre-multiplying the equation by transpose of n^{th} mode shape vector and then post multiplying the result by the n^{th} mode shape vector, using orthogonality of mode shapes with respect to the mass and stiffens matrices, we shall obtain

(3.9)

Now we must divide the equation to the critical damping coefficient of n^{th} mode, equals , final relation of Rayleigh damping, calculating n^{th} mode's damping ratio will be like the following equations.

(3.10)

(3.11)

Consider two modes, i^{th} *and* j^{th}, assume equal damping ratio for both, for example 5% damping ratio, and solving for two coefficients in the preceding equation, we'll have [39]:

(3.12)

(3.13)

By applying this procedure for modeling, method of selecting "*i*" and "*j*" are important. Chopra takes an example for this. Assume that we are going to take only

first five mode of vibration in to account, then we set *i* equals 1 and *j*, 4. As is shown in Figure 3.22, 2nd and 3rd mode's damping will be less than the specified ξ for 1st and 4th, while damping ratio of the 5th mode is greater than ξ, higher modes after the 5th, has negligible effect due to large damping.

Cross-sectional properties of the members of 3 and 9-story frames are presented in Tables 3.7 and 3.8, respectively.

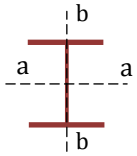

Table 3.7: Cross sectional properties of members of 3 story frame – SF3

Section	Section Tag	A (in^2)	d (in)	t_w (in)	b_f (in)	t_f (in)	I_a (in^4)
	2	91.4	17.12	1.41	16.230	2.260	4330
	1	75.6	16.38	1.175	15.995	1.890	3400
	-	20	14.04	0.415	10.035	0.720	723
	3	34.7	32.86	0.550	11.480	0.740	5900
	4	34.2	30.01	0.565	10.495	0.850	4930
	5	20.1	23.73	0.415	8.065	0.585	1830
	-	10.3	17.70	0.300	6.00	0.425	510
	-	7.68	15.69	0.250	5.500	0.345	301

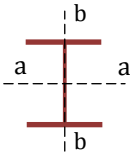

Table 3.8: Cross sectional properties of members of 9 story frame – SF9

Section	Section Tag	A (in2)	d (in)	tw (in)	bf (in)	tf (in)	Ia (in4)
		147	19.60	2.190	17.010	3.500	8210
		134	19.02	2.015	16.835	3.210	7190
		109	17.92	1.655	16.475	2.660	5440
		83.3	16.74	1.290	16.110	2.070	3840
		75.6	16.38	1.175	15.995	1.890	3400
		68.5	16.04	1.070	15.890	1.720	3010
		47.0	36.01	0.650	12.00	1.020	9750
		39.7	35.55	0.600	11.950	0.790	7800
		26.4	29.53	0.470	10.40	0.610	3620
		24.8	26.71	0.460	9.960	0.640	2850
		20.1	23.73	0.415	8.065	0.585	1830

Framing plan and orientation of columns in plan of frames are presented in Figure 3.24. Also, geometry of 3 and 9-story frames are shown in Figures 3.25 and Figure 3.26, respectively.

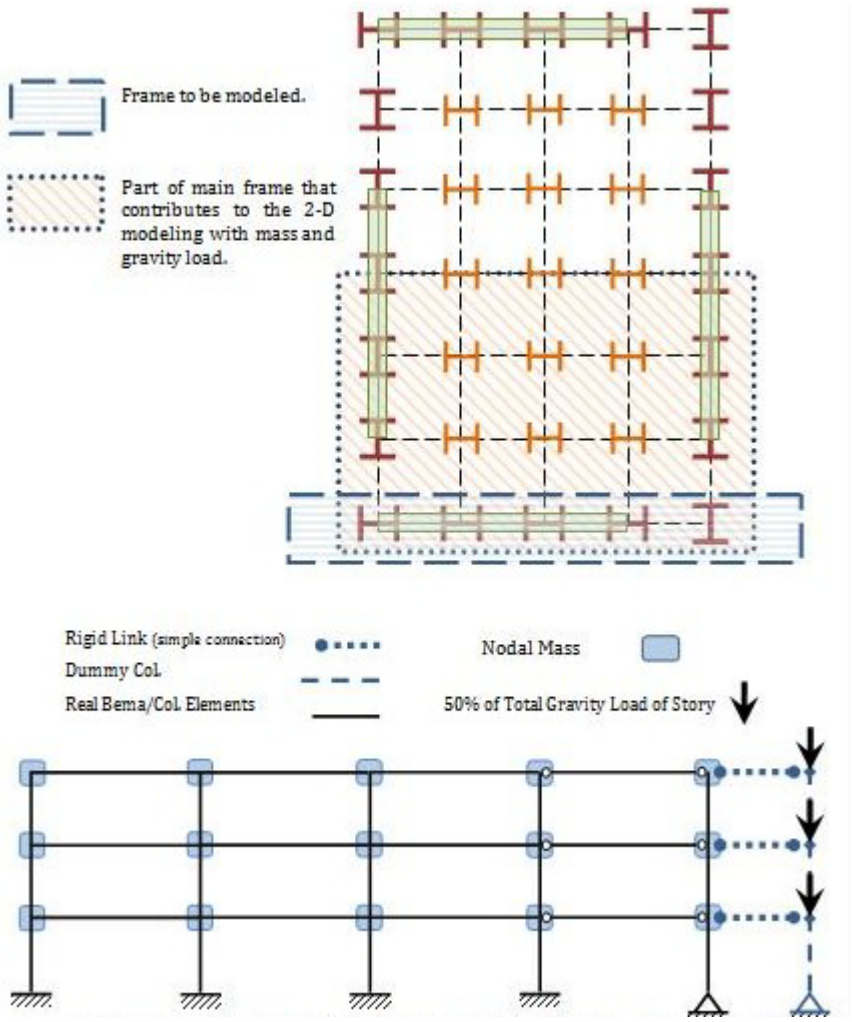

Figure 3.23: Schematic of 3-story frame with nodal mass, dummy load and gravity load applied.

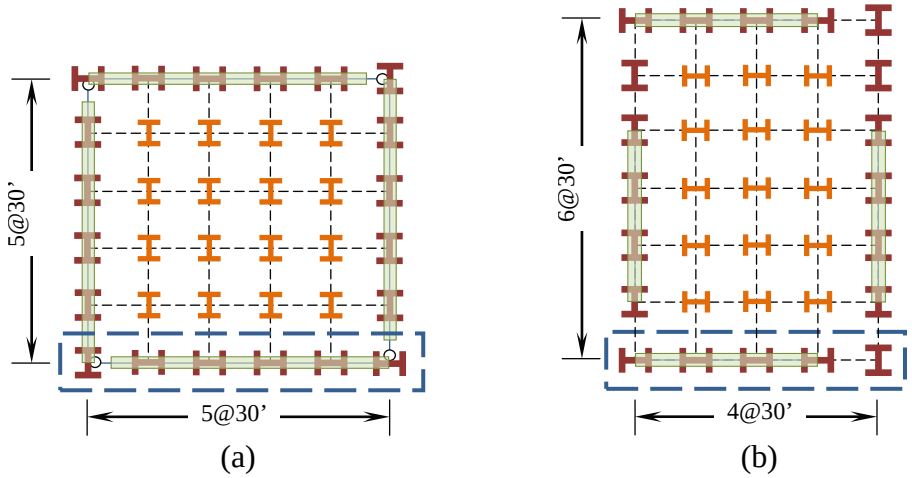

Figure 3.24: Framing plan and orientation of columns in plan of frames (a) nine story frame, (b) three story frame.

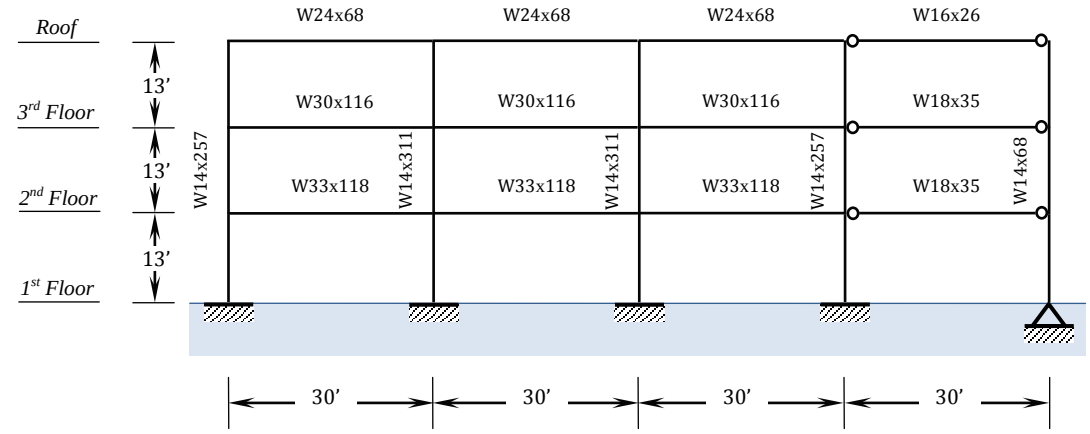

Figure 3.25: Geometry of 3 – story frame

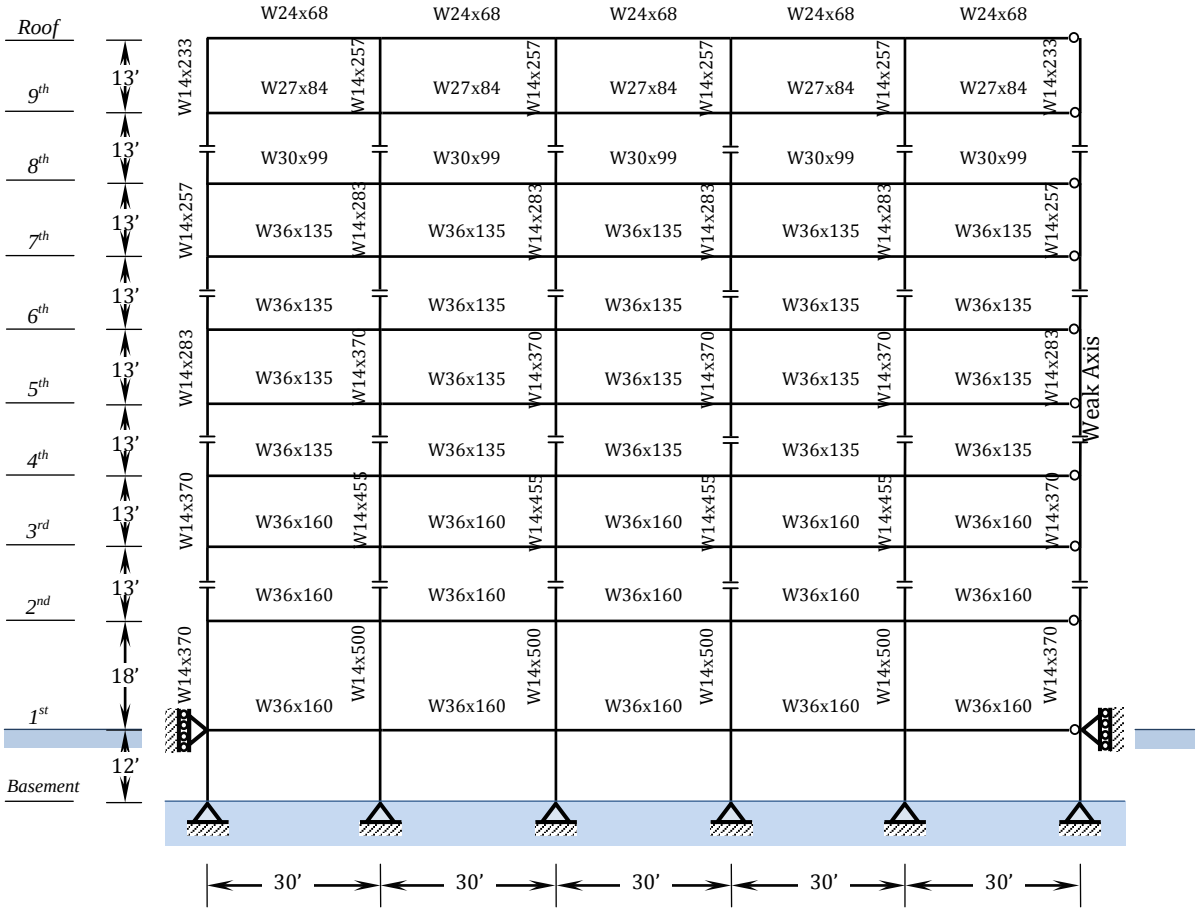

Figure 3.26: Geometry of 9– story frame

3.6 Considerations in Modeling of Beams, Columns and Dummy Columns by OpenSEES

Modeling of moment resisting frame buildings consists of modeling of beams, columns and their inelastic behavior. Figure 3.27 illustrates bending in beam and columns of a moment resisting frame. While maximum bending occurs at end points, and formation of plastic hinges at element end points make bending moment at the member ends to be constant, generally nonlinear modeling for of elements in MRFs needs the ability of formation of hinges only at element end points. Although formation of plastic hinges in end points is sequenced in constant bending moment, however deformation demands, it means rotation at plastic hinges keeping increasing. This cause end point plastic hinges to lengthen more and more. In other word plasticity or nonlinearity will propagate in the element length. FEMA355-F [40], based on notes from Gupta and Krawinkler proposed that using two zero length plastic hinges in modeling of beams is satisfactory, however it is not suitable for modeling of columns, especially due to presence of high axial load which may lead to occurrence of maximum bending moment in a point far different from column end points due to second order moments. So it should be stated that in Figure 3.27 distribution of moment is only due to application of lateral loads and p-delta effects are not considered. Consequently modeling of columns needs the ability to capture distributed nonlinearity rather than localized, as proposed for beams [30].

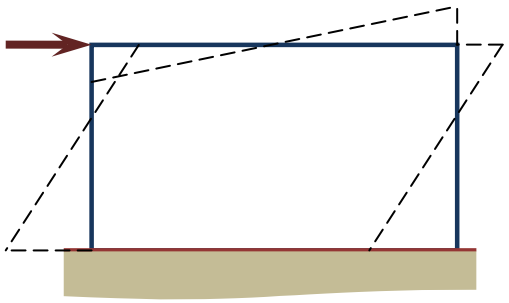

Figure 3.27: Schematic bending-moment diagram for a moment resisting frame due to local lateral load

Figure 3.28 shows a beam with two adjacent columns. Modeling of beam includes modeling of central elastic part and two zero length parts at end points. As this, each beam is modeled using four nodes, each pair at the same location. The elastic part is modeled using "elasticBeamColumn" model in OpenSEES. This model needs that Area (A), Modulus of Elasticity (E) and moment of inertia of section to be specified. At each end of central element, we will have two same-location nodes, to one, elastic beam is attached and to the other columns are connected. Connection of each pair is done via "zerolengthSection" command in OpenSEES. It needs the zero length section to be specified. As this, combination of a nonlinear fiber section for moment and two high stiffness elastic axial and shear links is used. It seems to be important to state that while a dummy column is connected to the main frame, and then it will transmit a series of considerably high horizontal load due to P-Delta effects to the frame, axial stiffness of beams must be in conformance with "rigid diaphragm" concept, otherwise axial elongation of beam rather formation of plastic hinges may cause high story drifts. Axial action of slabs in a real frame may cause nodes at one story to move horizontally in a same magnitude. Since our modeling is 2-D one, the most simple way is to define a very large value for area of elastic beam and high stiffness in axial action for two zero length end elements. Also for these two end connections, it shall be no interaction between axial and moment action [34].

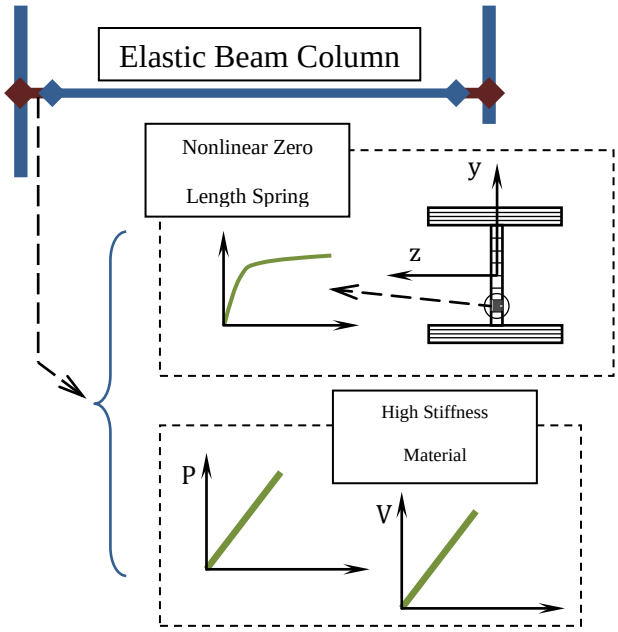

Figure 3.28: Modeling of a schematic beam with two adjacent columns in OpenSEES

Rather than the proposed technique for modeling of beams, which localizes plastic hinges at end points, modeling of columns due to their considerable amount of axial force, needs general or "distributed" plasticity models for elements, while nonlinearity may propagate in element length and P-Delta may cause the maximum moment to occur at a point different from end points (see Figure 3.29). As this, we will use "nonlinearBeamColumn" element model for columns. This model uses more than two integration points, in each, integration of response is conducted and then element response is determined using integration of responses in sections along the element. Although, yet we cannot capture problems raised from local phenomena such as local buckling.

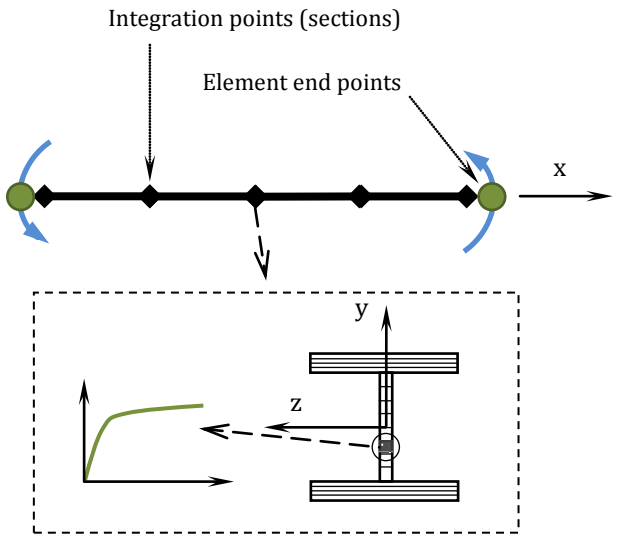

Figure 3.29: Integration points for a “nonlinearBeamColumn” element modeled for columns

In both zero length sections in beams, or full nonlinear element for columns, we have used fiber section to model bending action as shown in Figures 3.28 and 3.29. Fiber sections consist of fibers, generally with axial action only and without shear interaction. Combination of this action cause axial and bending action of section. To perform this, and especially for bending action, prediction of strain is needed. As this, OpenSEES utilizes linear distribution of strain along the element section [34]. Assuming plain remains plain after deformation due to strain linear variation (Figure 3.30), local phenomena such as local buckling in web or flanges (Figure 3.31) cannot be captured, and it is one of the most important drawbacks of our modeling.

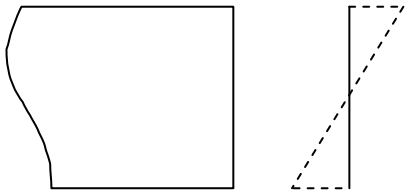

Figure 3.30: Strain distribution along all element sections

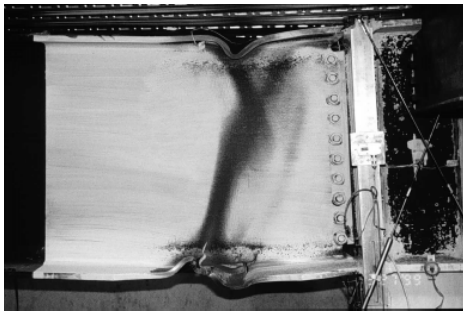

Figure 3.31: Local buckling phenomena in web and flanges

3.7 Stiffness Matrix of Two-Dimensional Fiber Element

Figure 3.32 illustrates the 2-D fiber element utilized in this research. The nonlinearity of the element is computed at the elemental middle cross section discrete into a number of fibers designated n_f. Each of the fibers is assigned a uniaxial constitutive model corresponding to a material it represents [41].

Incremental axial strain at the centroid, $\Delta\varepsilon_a$, and incremental curvature, $\Delta\phi$, of a fiber element between time t and $t+\Delta t$ are given as:

(3.14)

(3.15)

Where L is the element length, Δu_i and Δu_j are the incremental end displacements at i end and j end, respectively.

Employing the assumptions of plane section remaining plane after deformation as illustrated in Figure 3.33, the incremental strains of the k-th fiber can be obtained as:

(3.16)

Where y_k is the distance from the centroid to the reference point of the k-th fiber. The area of the k-th fiber, A_k, and tangent stiffness, E_{kt} (which is obtained from strain state in each fiber at time t), can be used to obtain the element incremental axial force and bending moment between time t and $t+\Delta t$:

(3.17)

(3.18)

(3.19)

(3.20)

(3.21)

In matrix form, the relationship between the incremental end forces, $\{\Delta f\}$, and the incremental end displacements, $\{\Delta u\}$, can be written as:

(3.22)

(3.23)

(3.24)

Assuming the deformed shape of the element as

$$u(x) = c_0 + c_1 x \tag{3.25}$$

$$v(x) = c_2 + c_3 x + c_4 x^2 - c_5 x^3 \tag{3.26}$$

Therefore, the stiffness matrix of 2-D fiber element, $[k_t]$, is expressed as follow:

$$[k_t] = \begin{bmatrix} \frac{EA_t^*}{L} & 0 & -\frac{EG_t^*}{L} & -\frac{EA_t^*}{L} & 0 & \frac{EG_t^*}{L} \\ 0 & \frac{12EI_t^*}{L^3} & \frac{6EI_t^*}{L^2} & 0 & -\frac{12EI_t^*}{L^3} & \frac{6EI_t^*}{L^2} \\ -\frac{EG_t^*}{L} & \frac{6EI_t^*}{L^2} & \frac{4EI_t^*}{L} & \frac{EG_t^*}{L} & -\frac{6EI_t^*}{L^2} & \frac{2EI_t^*}{L} \\ -\frac{EA_t^*}{L} & 0 & \frac{EG_t^*}{L} & \frac{EA_t^*}{L} & 0 & -\frac{EG_t^*}{L} \\ 0 & -\frac{12EI_t^*}{L^3} & -\frac{6EI_t^*}{L^2} & 0 & \frac{12EI_t^*}{L^3} & -\frac{6EI_t^*}{L^2} \\ \frac{EG_t^*}{L} & \frac{6EI_t^*}{L^2} & \frac{2EI_t^*}{L} & -\frac{EG_t^*}{L} & -\frac{6EI_t^*}{L^2} & \frac{4EI_t^*}{L} \end{bmatrix} \tag{3.27}$$

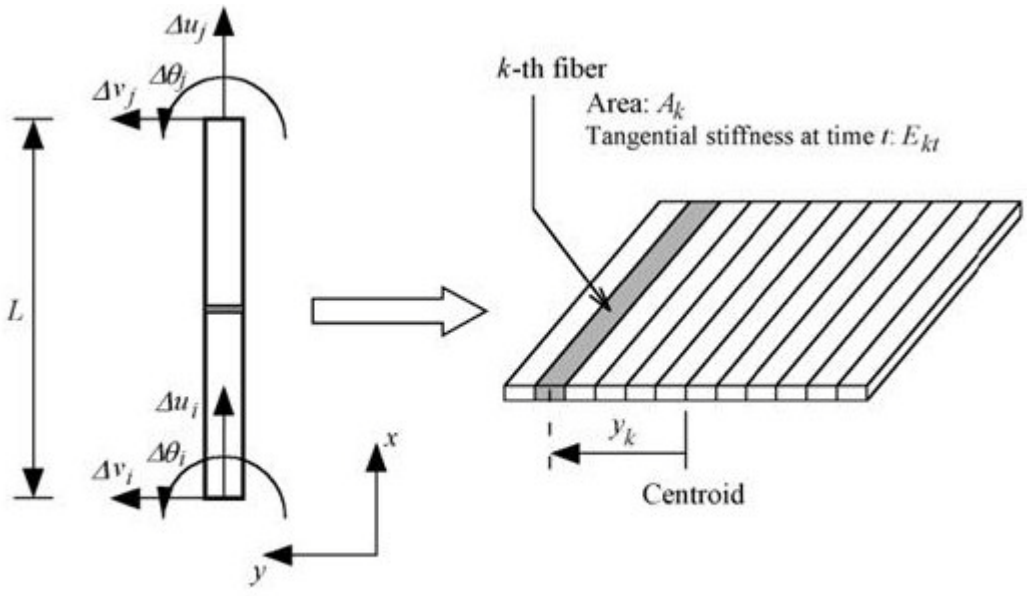

(a) Two-dimensional fiber element (b) Fiber section at the middle of element

Figure 3.32: Fiber element

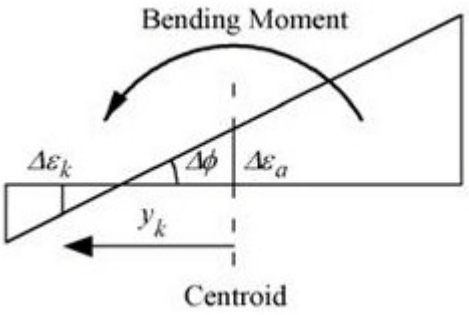

Figure 3.33: Incremental axial strain of *k*-th fiber

3.8 Fracture

The fatigue material uses a modified rain-flow cycle counting algorithm to accumulate damage in a material using Miner's rule. Element stress-strain relationships become zero when fatigue life is exhausted.

uniaxialMaterial fatigue $matTag $tag <-E0 $E0> <-m $m> <-max $max>

This material model accounts for the effects of low cycle fatigue. A modified rain-flow cycle counter has been implemented to track strain amplitude. This cycle counter is used in counter with a linear strain accumulation model (i.e. Miner's rule), based on Coffin-Manson log-log relationship describing low cycle fatigue failure. This material "wraps" around another material and does not influence the stress-strain (or force-deformation) relationship of the parent material.

Once the fatigue material model reaches a damage level of 1.0, the force (or stress) of the parent material becomes zero. If failure is triggered in compression, the material stress is dropped at the next zero-force crossing (i.e. compression force never "drops" to zero).

The fatigue material assumes that each point is the last point of the history and tracks damage with this assumption. If failure is not triggered, this pseudo-peak is discarded.

The material also has the ability to trigger failure based on a maximum or minimum strain (i.e. not related to fatigue). The default for these values is set to very large numbers.

The default values are calibrated parameters from low cycle fatigue tests of European steel sections Ballio and Castiglioni (1995), for more information about how material was calibrated, the user is directed to Uriz (2005).

$matTag: Unique material object integer tag
$tag: Unique material object integer tag for the material that is being “wrapped”
$E0: Value of strain at which one cycle will cause failure (Default 0.191)
$m: Slope of Coffin-Manson curve in log-log space (default 0.458)
$min: Global minimum value for strain or deformation
$max: Global maximum value for strain or deformation [34]

While we are using fiber sections as the nonlinear part of our modeling, fracture is generally defined at the level of fibers. Nonlinear behavior of steel structures is included with damage due to low cycle fatigue. Fatigue in a general term is to form and propagation of micro cracks in the cross section due to repetition of load, till the un-cracked section cease its stability to support the applied load and afterward it will completely diminished.

Fatigue problems are common whenever cyclic load present. If loading cause the element to behave in elastic range, huge numbers of repetition is needed to cause fatigue problems to fail the cross section at load levels lower than its nominal strength. As this, fatigue problems in elastic range are called high cycle fatigue. In contrast, if element behave in its nonlinear range, fatigue cause fracture in "deformation" less than nominal fracture deformation. In this range number of cycles needed is at the order of 10 to 20 (rather than high cycle in which number of needed cycles was at order 10^4 to 10^6). So, we call it low cycle fatigue.

Fatigue tests are performed at constant strain or stress for elastic and inelastic behavior test respectively, and their result is number of cycles needed to cause at that amplitude. So, number of cycles to failure in each case is a function of amplitude of stress or strain. Our discussion here is low cycle fatigue therefore, here we only discuss about amplitude.

As number of cycles needed to cause failure is function of strain amplitude, we may fit an analytical curve on data achieved. This is down using Coffine-Manson relation.

In real loading situation, we never face constant amplitude cycles of strain or stress, but results from fatigue tests are usually based on constant amplitude of strain. So, we need to combine test data to gain reasonable procedure on assessment of low cycle fatigue life of a fiber. This is done by using Miner rule. It linearly combine damage took place at each step of loading. Damage at each step assumes to be ratio of number of cycles at a specified strain value, to the number of cycles needed to fracture at that strain in constant amplitude test. Miner rule add these damage values

in a linear manner and calls it the Damage Index. Whenever DI reaches one, the corresponding fiber will be omitted in calculation of strength of the section.

(3.28)

(□) = exp(— — (3.29)

Damage Index based on Miner rule is:

——— (3.30)

Calculate *DI*: if it is less than 1.0, fatigue does not occur otherwise, fracture takes place.

Finally Patix Uriz calibration, $\square_0$ = 0.191 and *m*= -0.458 are used and also maximum allowable strain of 0.090 will be applied to the fibers according to the experimental tests done on steel material [42], [43].

Chapter 4

METHODOLOGY

4.1 Introduction

This chapter focuses on the step by step methodology of the analysis approach of collapse control, ground motion selection as well as the probabilistic approach in detail and the related documents utilized based on the model considerations discussed in Chapter 3.

4.2 Collapse Investigations

Present study is focused on two 3-story and 9-story steel moment resisting frames introduced in detail in Chapter 3. Generally the aim is to apply incremental dynamic analysis on them. That is, each accelerograph is scaled from lower levels and incrementally increased to the level in which collapse occurs.

Collapse in this study refers to the unlimited sidesway. When the frame experiences sidesway, the gravity loads applied on dummy column will cause second order P-Δ effect and this will produce axial loads in links as shown in Figure 4.1.

When the axial loads in links become greater than the lateral capacity of frame, the structure becomes unstable and it will experience “Rigid Body Motion”. In other words, it has unlimited side sway discussed above.

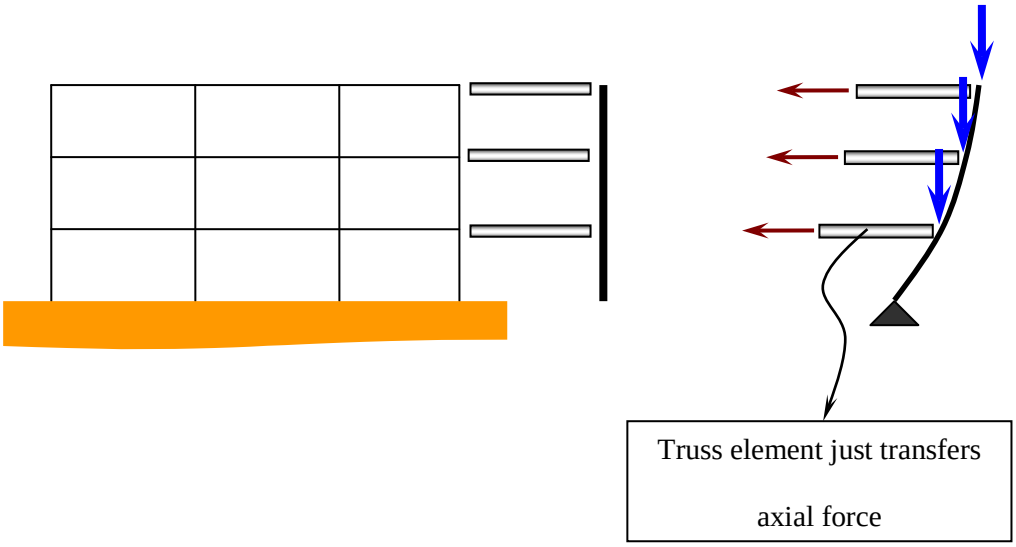

Figure 4.1: Dummy column and truss element links for transferring axial loads due to P-Δ effect

In order to control a limit point for “unlimited sidesway” in OpenSEES, during running the program by the application of ground motion excitation, at each time interval the displacement at each level is read and the relative displacement of two upper and lower story of that level with respect to that point is calculated and if it is greater than 10% of the height of corresponding story, then it will stop analysis and says “Collapse Occurs”. Otherwise, Maximum drift ratio is recorded as the corresponding maximum drift ratio to that level of excitation and then the accelerograph will be increased gradually and the analysis will continue with a higher PGA until “Collapse Occurs”. The “PGA[g]” versus “Maximum inter-story drift ratio [%]” curve for each ground motion is identified.

The below script sample is what has been written in OpenSEES software to control the Collapse according what is expressed above:

set Allowable_Drift [expr 12*13*0.1]: # story height is 13 ft = 12*13 inch. Consider understory drift as collapse.

```
set dt 0.01: #record dt (time intervals between earthquake records)
set NPT 2500: #record number of points (number of earthquake time intervals)
# performing analysis.
# We can write “analyze $NPT $dt” instead of defining for, but we need displacement at each time interval to check collapse.
for {set ii 1} {$ii <= $NPT} {incr ii} {
        analyze 1 $dt
        set D1 [nodeDisp 204 1]
        set D2 [nodeDisp 304 1]
        set D3 [nodeDisp 404 1]
        set DR1 [expr abs($D1)]
        set DR2 [expr abs($D2-$D1)]
        set DR3 [expr abs($D2-$D3)]
        set D_Cu [expr max($DR1,$DR2,$DR3)]
        if {$D_Cu >= $Allowable_Drift
                puts
                puts"###### COLLAPSED!!!! at $ii #########”
                puts
                set DR_MAX $D_Cu
                set STATE "Collapsed ：
                return -1          # it breaks the analysis loop.
        }
}
```

As it was mentioned above, if 10% of height of story is obtained, the analysis is stopped and it says “Collapse occurs”. 10% is a suitable value for our structures

because it’s much more than allowable maximum drift ratio recommended by the specifications that is 4% for collapse state and as it was discussed in Chapter 3. So, if 10% drift ratio occurs, somehow, it is concluded that rigid body motion took place, therefore the lateral capacity has been diminished severely and in other word, collapse occurs.

4.3 Ground Motion Selection

Application of Incremental Dynamic Analysis involves a series of nonlinear dynamic time-history analyses, thus it is essential to have a suitable ground motion record series. Ground motion selection for time-history analysis is a very complicated task since they will have different effects on structural response due to differences in their characteristics. In addition to this, since the accuracy of IDA results are affected by number of selected ground motions, this issue becomes more complicated.

In the research, done by Curt B. Haselton, he developed a general far-field ground motion set for use in structural analyses and performance assessment. This ground motion set includes the 22 pair of horizontal ground motions that comprise the FEMA P695 (ATC-63) has more extensive documentation that is available in Table 4.1.

This ground motion set is called “Basic Far-Field Set” or “Set FFext” was selected to consist of strong motions that may cause structural collapse of modern buildings. This typically occurs at extremely large levels of ground motion, so this ground motion set was selected to represent these extreme motions to the extent possible.

To insure that the records represent strong motion that may cause structural collapse, minimum limits on event magnitude as well as peak ground velocity and acceleration

were imposed. The limits were chosen to balance selection of large motions, while insuring that enough motions will meet the selection criteria [44]:

- Magnitude > 6.5
- Distance from source to site > 10 km (average of Joyner-Boore and Campbell distances)
- Peak ground acceleration > 0.2g
- Peak ground velocity > 15 cm/sec
- Soil shear wave velocity, in upper 30m of soil, greater than 180m/s (NEHRP soil type A-D: note that all selected records happened to be on C/D sites)
- Limit of six records from a single seismic event: if more than six records pass the initial criteria, then the six records with largest PGV are selected, but in some cases a lower PGV record is used if the PGA is much larger
- Lowest usable frequency < 0.25Hz, to ensure that the low frequency content was not removed by the ground motion filtering process
- Strike-slip and thrust faults (consistent with California)
- No consideration of spectral shape
- No consideration of station housing, but PEER-NGA records were selected to be “free-field”

Table 4.1: Twenty two pairs of Ground Motions selected utilized for analyses

			Event Information				Site Information				Record Information		
EQ Index	**EQ ID**	**PEER-NGA Rec. Num.**	**Mag.**	**Year**	**Event**	**Fault Type**	**Station Name**	**Vs_30 (m/s)**	**Campbell Distance (km)**	**Joyner-Boore Distance (km)**	**Lowest Useable Freq. (Hz)**	**Horizontal Acceleration Time History Files**	
1	12011	953	6.7	1994	Northridge	Blind thrust	Beverly Hills	356	17.2	9.4	0.25	NORTHR/MUL009.at2	NORTHR/MUL279.at2
2	12012	960	6.7	1994	Northridge	Blind thrust	Canyon Country	309	12.4	11.4	0.13	NORTHR/LOS000.at2	NORTHR/LOS270.at2
3	12041	1602	7.1	1999	Duzce, Turkey	Strike-slip	Bolu	326	12.4	12.0	0.06	DUZCE/BOL000.at2	DUZCE/BOL090.at2
4	12052	1787	7.1	1999	Hector Mine	Strike-slip	Hector	685	12.0	10.4	0.04	HECTOR/HEC000.at2	HECTOR/HEC090.at2
5	12061	169	6.5	1979	Imperial Valley	Strike-slip	Delta	275	22.5	22.0	0.06	IMPVALL/H-DLT262.at2	IMPVALL/H-DLT352.at2
6	12062	174	6.5	1979	Imperial Valley	Strike-slip	El Centro Array #11	196	13.5	12.5	0.25	IMPVALL/H-E11140.at2	IMPVALL/H-E11230.at2
7	12071	1111	6.9	1995	Kobe, Japan	Strike-slip	Nishi-Akashi	609	25.2	7.1	0.13	KOBE/NIS000.at2	KOBE/NIS090.at2
8	12072	1116	6.9	1995	Kobe, Japan	Strike-slip	Shin-Osaka	256	28.5	19.1	0.13	KOBE/SHI000.at2	KOBE/SHI090.at2
9	12081	1158	7.5	1999	Kocaeli, Turkey	Strike-slip	Duzce	276	15.4	13.6	0.24	KOCAELI/DZC180.at2	KOCAELI/DZC270.at2
10	12082	1148	7.5	1999	Kocaeli, Turkey	Strike-slip	Arcelik	523	13.5	10.6	0.09	KOCAELI/ARC000.at2	KOCAELI/ARC090.at2
11	12091	900	7.3	1992	Landers	Strike-slip	Yermo Fire Station	354	23.8	23.6	0.07	LANDERS/YER270.at2	LANDERS/YER360.at2
12	12092	848	7.3	1992	Landers	Strike-slip	Coolwater	271	20.0	19.7	0.13	LANDERS/CLW-LN.at2	LANDERS/CLW-TR.at2
13	12101	752	6.9	1989	Loma Prieta	Strike-slip	Capitola	289	35.5	8.7	0.13	LOMAP/CAP000.at2	LOMAP/CAP090.at2
14	12102	767	6.9	1989	Loma Prieta	Strike-slip	Gilroy Array #3	350	12.8	12.2	0.13	LOMAP/G03000.at2	LOMAP/G03090.at2
15	12111	1633	7.4	1990	Manjil, Iran	Strike-slip	Abbar	724	13.0	12.6	0.13	MANJIL/ABBAR--L.at2	MANJIL/ABBAR--T.at2
16	12121	721	6.5	1987	Superstition Hills	Strike-slip	El Centro Imp. Co. Cent	192	18.5	18.2	0.13	SUPERST/B-ICC000.at2	SUPERST/B-ICC090.at2
17	12122	725	6.5	1987	Superstition Hills	Strike-slip	Poe Road (temp)	208	11.7	11.2	0.25	SUPERST/B-POE270.at2	SUPERST/B-POE360.at2
18	12132	829	7.0	1992	Cape Mendocino	Thrust	Rio Dell Overpass - FF	312	14.3	7.9	0.07	CAPEMEND/RIO270.at2	CAPEMEND/RIO360.at2
19	12141	1244	7.6	1999	Chi-Chi, Taiwan	Thrust	CHY101	259	15.5	10.0	0.05	CHICHI/CHY101-E.at2	CHICHI/CHY101-N.at2
20	12142	1485	7.6	1999	Chi-Chi, Taiwan	Thrust	TCU045	705	26.8	26.0	0.05	CHICHI/TCU045-E.at2	CHICHI/TCU045-N.at2
21	12151	68	6.6	1971	San Fernando	Thrust	LA - Hollywood Stor	316	25.9	22.8	0.25	SFERN/PEL090.at2	SFERN/PEL180.at2
22	12171	125	6.5	1976	Friuli, Italy	Thrust	Tolmezzo	425	15.8	15.0	0.13	FRIULI/A-TMZ000.at2	FRIULI/A-TMZ270.at2

After selection of ground motions that satisfy the criteria discussed above, it's needed to apply these records to our Steel Moment Resisting Frames. So, next part how to scale ground motions in order to obtain maximum inter-story drift ratio and finally drawing IDA curves.

4.4 Scaling of Ground Motion Records

Next issue after preparing the model and selecting the earthquake ground motion records is to scale the records appropriately. Running an actual Incremental Dynamic Analysis needs series of scaled levels of an earthquake ground motion record to be applied to the structure model in a way that could cover the whole range of its behavior and response.

In present study, Intensity Measure levels are increased from 0.00g to the Intensity measure of collapse by incremental value of 0.05g. In more details, all of the records of earthquakes are scaled in a manner that the PGA becomes equal to IM_i according to Equation 4.1. So, the algorithm is as follow in order to encounter the first numerical non-convergence which signals the global instability:

(4.1)

Where:

IM_i = ith Intensity Measure

g = Gravity acceleration

c = Point indicates the first numerical non-convergence or in other words, point of collapse.

Therefore, IM_c is defined as the Intensity Measure that collapse takes place.

4.5 Post-processing and Generating IDA Curves

Selection of a proper Intensity Measurement (IM) is the most significant part of post-processing of the results. As it was discussed in part 4.3 there are 44 earthquake records that should be applied one be one to the desired Steel Moment Resisting Frames and each of them should be incrementally increased till collapse occurs according to Equation 4.1 expressed in section 4.4. All of the steps in order to do Incremental Dynamic Analysis are conducted automatically by the OpenSEES as it is expressed below. Two general files should be sounded together: first is the Model file includes model and time history analysis for a given record and second is the IDA algorithm sounded to Model file each time and performs time history analysis for all records, each of them “c” times (see Equation 4.1) up to collapse.

MODELING: it needs EQ record file, its dt and its NPT

Model is constructed

- Nodes
- Elements
- Gravity loads are applied

Dynamic Analysis is performed
Using EQ record

- Record time step (dt)
- Number of data Point in record (NPT)

```
Set STATE "successful"
Set DR_max 0

For ii=1:NPT    analysis performed for each time step
        Perform analysis        <analyze $dt>
        If analysis contains error
                Do some thing to achieve convergence
                        + change algorithm type
                        + decrease time step

        End

        Calculate max. drift at time ii

        IF (drift > allowable _ drift & converged)
                Collapse occurred
                Set state "collapsed"
                Set DR_max $allowable_drift

        Else if (drift > $DR_max & converged)
                Set DR_max $drift
        Else if (did not converge)
                Set state "non-converged"
        End
End

Return $DR_max & $State      it returns these two values to the main file
```

IDA ALGORITHM It is described step by step

1- Read records information file. It contains record name, its dt, NPT and PGA (According to table 4.1).

2- Perform analysis for each record

   a. Create an output folder for this record it contains two files;
      i. DR.txt this file contains max drift and/or value of IM up to collapse, for example we run 6 times to see collapse, so it has one (or two) column(s) of 6 numbers.

      ii. RE.txt this contains "state" parameter at each step. We use it to ensure there will be no non-converged case.

      So create DR.txt and RE.txt and both are null at start.

   b. Scale record to an arbitrary low level, for example 0.05g. All start with the same (According to equation 4.1).

   c. Sound MODEL_FILE.tcl and perform analysis using its dt & NPT. Read outputs from model file. Outputs are DR_max and state. "State" specifies that dose collapse reached or not

   d. Increase by 0.05, for example in the second step EQ level is 0.10g, and perform part c.
   e. Yet state is equal "successful", perform part d. it means that
      i. Increase EQ level
      ii. Sound model file
      iii. Read DR_max and put it in DR.txt
      iv. Read STATE and put it in RE.txt

   f. When state becomes "collapse" or "non-converged", analysis for current record is finished. No close DR.txt and RE.txt, and get ready for new record.

3- Go to part 2 and perform IDA for next record.

After analyzing two “Moment Resisting Steel Frames” (SMRF) by applying above algorithms, next issue is to draw IDA curves of IM_i versus Maximum Inter-story Drift Ratio for each earthquake record. After performing IDA and determining collapse IM, IM_c, putting a probability rule, Cumulative Distribution Function (CDF) of IM_c can be found. It is called “Fragility Curve”. This curve generally describes variation of responses due to input earthquakes. Fragility curves can contain variation of results due to variation in material properties, analysis algorithms Etc.

Fragility curves can be generated for each performance level. They are usually constructed based on response of frame, such as deformations, drifts and other responses, but for collapse it is more usual to use record properties: IM_c.

4.6 Fragility Curves

To obtain collapse fragility curves, it is proposed to use IM-based approach [1] rather than EDP- based [45]. Finding IM_c for each record, fragility curve means to obtain Cumulative Distribution Function, CDF. This CDF can be determined based on either a standard probability distribution (assume to be lognormal) or fraction based. These two CDFs are generally reported. It means that probability of any event is proportional to its frequency (n/N) where, n is the number of similar IM_cs and N is the total number of records. So, N is forty four in this research.

4.6.1 Log-Normal Distribution Function

Returns the cumulative Log-Normal distribution of x, where $ln(x)$ is normally distributed with parameters mean and standard deviation. The function that is used to analyze data has been transformed logarithmically [46].

(4.2)

Where:

x: The value at which to evaluate the function

μ: Mean of $ln(x)$

σ: Standard deviation

4.6.2 Fraction-Based Approach

In order to construct fragility curve by fraction-based method IM_cs obtained from IDA curves should be sorted from smallest to the largest values. Then, probability of each IM is n/N. For example, if there is three IM of 0.4g according to the analysis, n=3 and since there are forty four earthquake records, N=44. For IM_cs with similar values, P is constant. And finally, CDF is generated simply by adding P of IM_cs equal or greater than the specified.

4.7 Seismic Hazard Curve to Find MAF and Probability of Collapse

The seismic hazard curve is taken in to account as a link between the collapse fragility curve and seismic hazard associated with the ground motion IM considered in the collapse fragility curve. A seismic hazard curve is description of the ground motion intensity and is obtained by Probabilistic Seismic Hazard Analysis [1]. The place of structures is in Los Angeles so, according to the latitude and longitude of Los Angeles California [47], data points representing the seismic hazard curve for location of two moment-resisting steel frames can be utilized from USGS toolkit [48].

Using these data, power form will be applied as follows to data gained from USGS. Data points from USGS are $\lambda(PGA)$ versus PGA values. So, by applying power form, k_0 and k that will be found for place of Los Angeles, California [28].

(4.3)

After defining k_0 and k by using seismic hazard curve and putting in Equation 4.3., collapse data from IDA curves is needed. From IDA curves η_c (Equation 4.4), geometric mean (sometimes called "median"), as well as β_c (Equation 4.5), dispersion of collapse data are found as follow:

(4.4)

(4.5)

Where:

x_i: IM_c for each record

n: Total number of records

Finally, after defining k_0, k, η_c and β_c, by the use of Equation 4.6, λ_c can be found:

(4.6)

(4.7)

Where:

λ_c: Mean Annual Frequency of Collapse

$P[Collapse]$: Probability of collapse in 50 years [49]

Chapter 5 focuses on analyses and results of two SMRFs according to methodology discussed in current chapter.

Chapter 5

ANALYSES AND RESULTS

5.1 Introduction

This chapter concentrates on analyses and results of what were discussed in Chapter 4 based on the modeling considerations vastly remarked in Chapter 3. Briefly, in current chapter, there is one step by step example of generating IDA curve under the application of ground motion excitation due to Ground Motion scaling from lower level of *IM* to the IM_c that collapse occurs. Then the following issues are presented for both 3 and 9-story moment resisting steel frames; results of post-processing and IDA curves related to forty four earthquake records, fragility curves, seismic hazard curve of "return period of 5% in 50 years" for the place of "Los Angeles, California" and finally estimating the probability of collapse according to Mean Annual Frequency.

5.2 Generating IDA Curve for EQ Index 12012(1) Applied on 9-story SMRF

This part is related to the application of earthquake record index 12012(1) (see Table 4.1 for event, site and record information) on 9-story SMRF in order to find IDA curve.

dt= 0.01

N= 1999

PGA(g) = 0.831528234

Figures 5.1 to 5.4 show the scaled ground motions to 0.15, 0.30, 0.60 and 0.75 respectively.

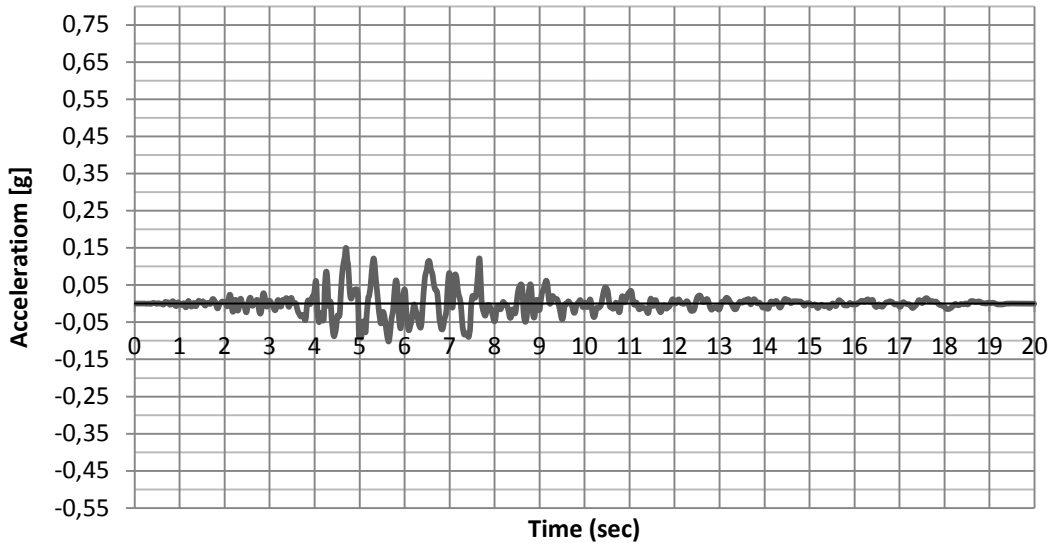

Figure 5.1: Scaled EQ to the 0.15[g]

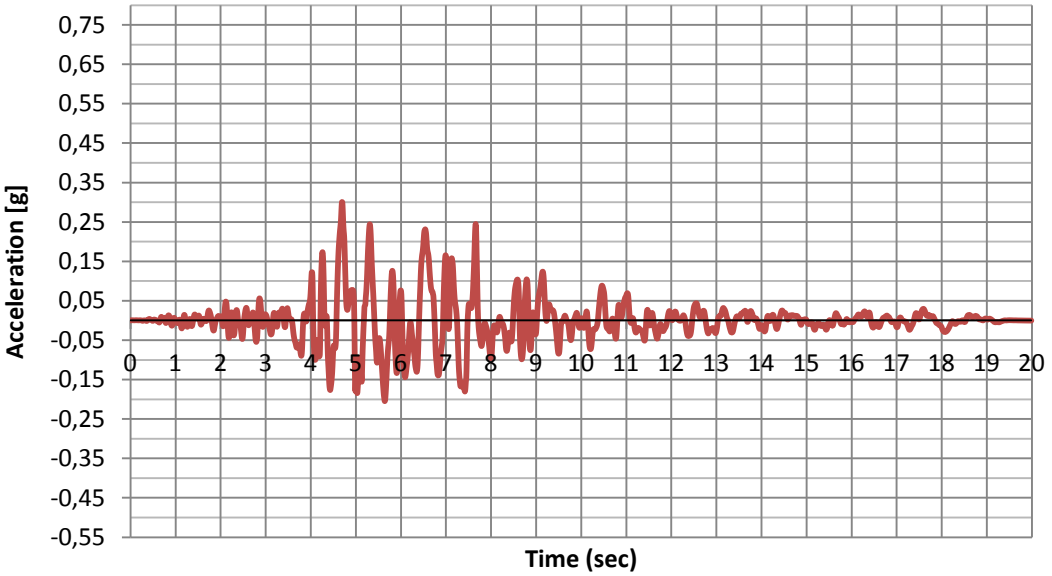

Figure 5.2: Scaled EQ to the 0.30[g]

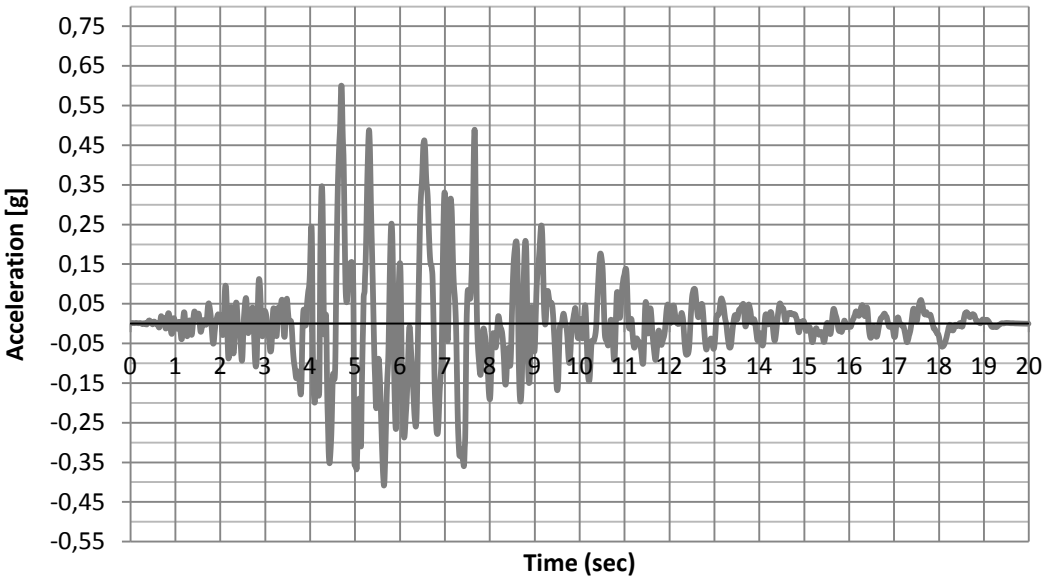

Figure 5.3: Scaled EQ to the 0.60[g]

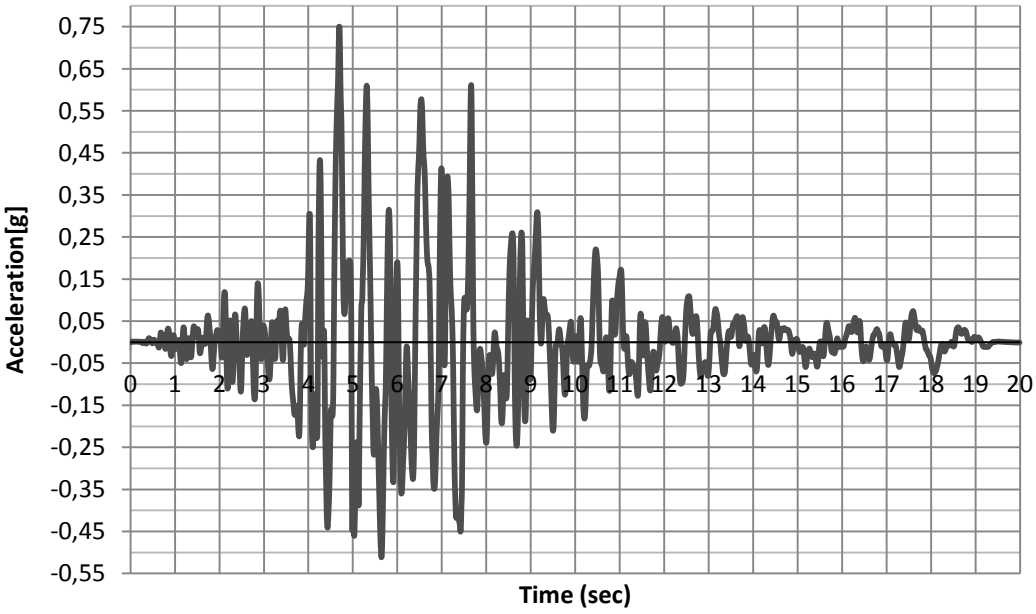

Figure 5.4: Scaled EQ to the 0.75[g]

As it was discussed in part 4.4, Intensity measure levels are increased by the value of 0.05g (see Equation 4.1) until global collapse occurs. Therefore, Figures 5.1 to

Figure 5.4 are some IMs that are applied to the structure in order to generate IDA curve. Table 5.1 and Figure 5.5 are the Maximum Drift corresponding to IMs and IDA curve related to specified earthquake applied on 9-story SMRF. Triangles shown on Figure 5.5 are the IMs those scaled ground motions are plotted in Figure 5.1 to Figure 5.4.

Table 5.1: Results of Time History Analysis of EQ 12012(1) applied on 9-story SMRF

IM (PGA) [g]	Drift (Inch)	MIDR [%]
0.00	0.00	0.00
0.05	0.27	0.17
0.10	0.54	0.35
0.15	0.81	0.52
0.20	1.08	0.69
0.25	1.35	0.86
0.30	1.61	1.03
0.35	1.86	1.19
0.40	2.09	1.34
0.45	2.28	1.46
0.50	2.43	1.56
0.55	2.66	1.70
0.60	3.09	1.98
0.65	3.61	2.31
0.70	4.25	2.72
0.75	15.60	10.00

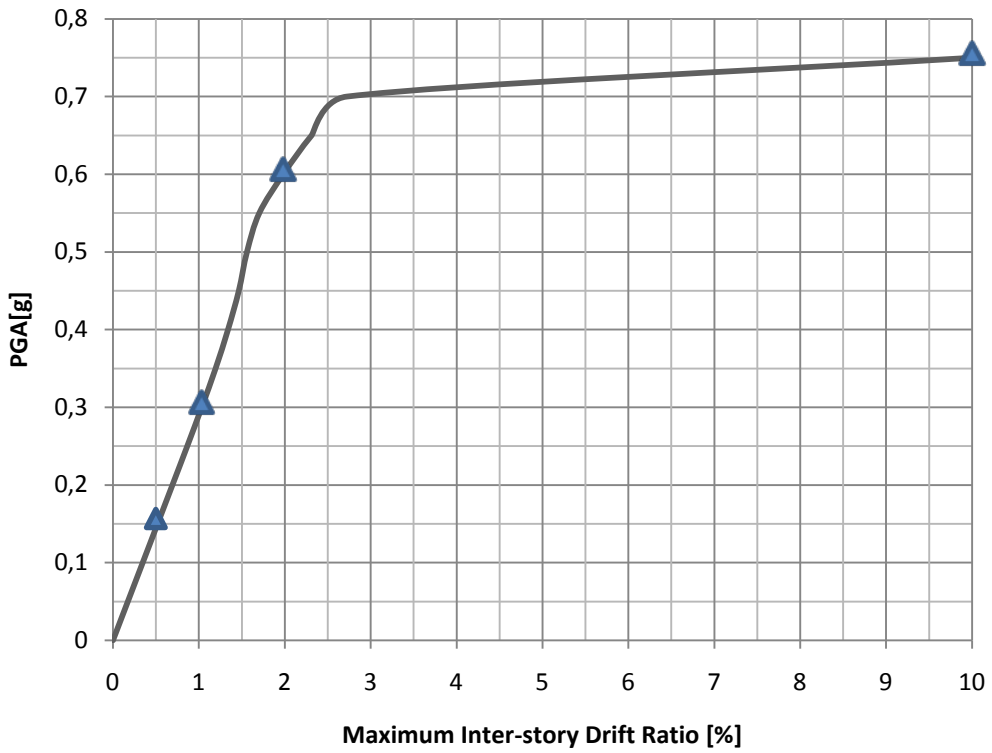

Figure 5.5: IDA curve related to Time History Analysis due to EQ 12012(1) applied on 9-story SMRF

5.3 Multi-Records IDA Curves

Following previous sections, now multi-record IDA curves can be plotted corresponding to the forty four extracted single IDA curves for each earthquake ground motion record as shown in Figure 5.6 and Figure 5.7 for three and nine story moment resisting steel frames, respectively. Note that first, second and third modes are taken into consideration in order to find maximum inter-story drifts and the values of Natural Circular Frequencies are 1.44sec, 0.338sec and 0.174sec for the 3-story SMRF and 1.365sec, 0.807sec and 0.457sec for the 9-story SMRF respectively.

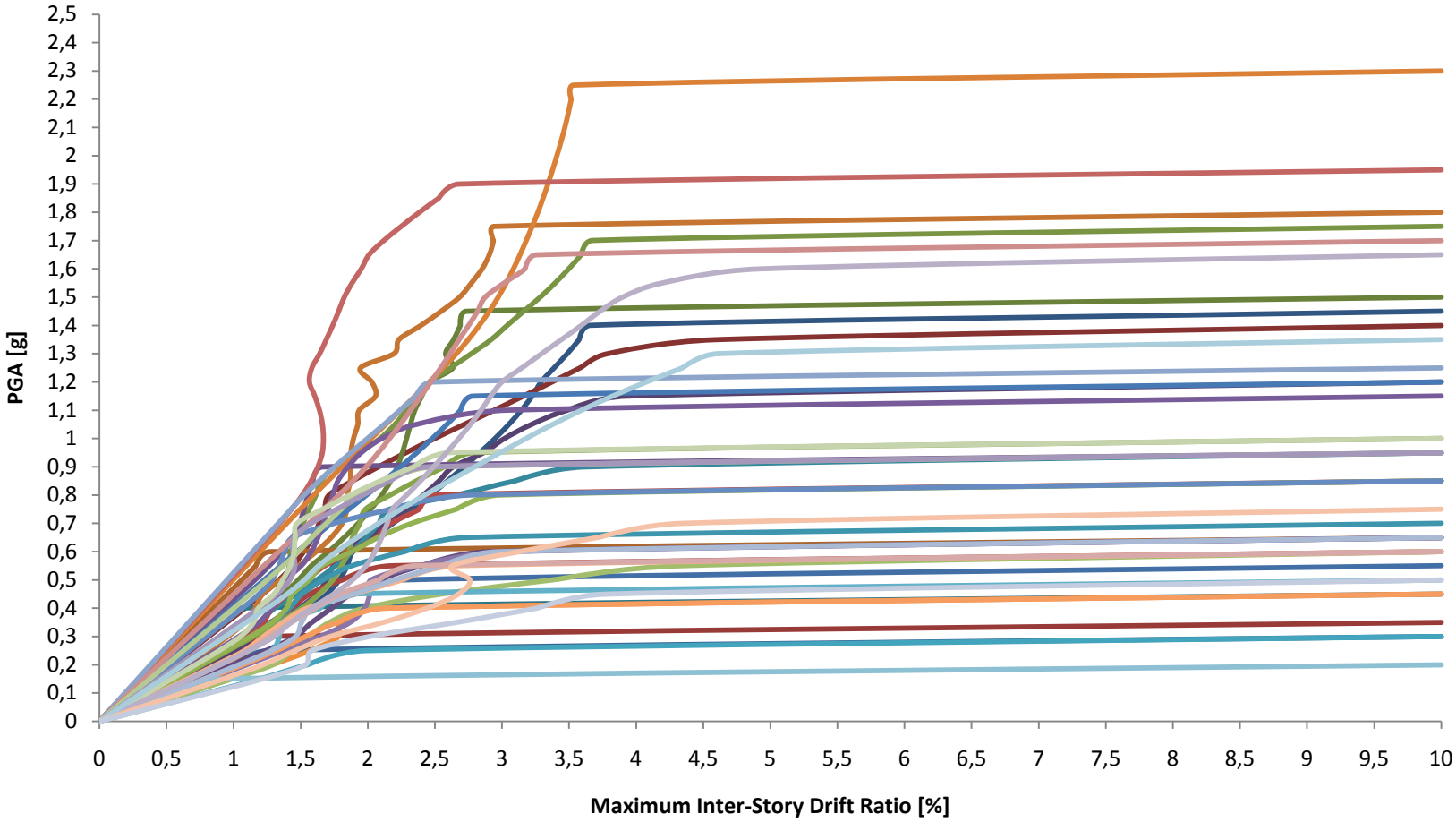

Figure 5.6: IDA curves of forty four earthquakes for 3-story SMRF

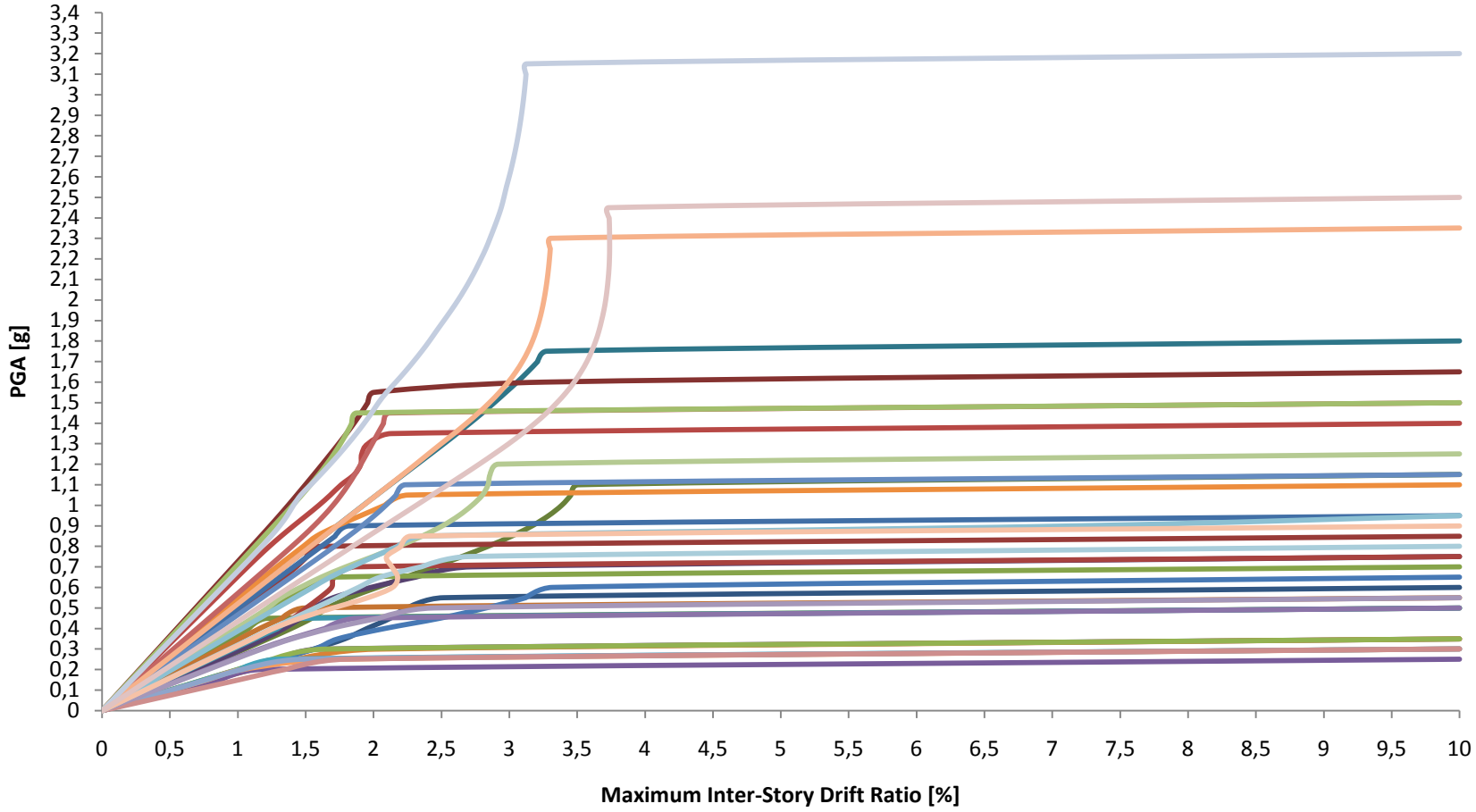

Figure 5.7: IDA curves of forty four earthquakes for 9-story SMRF

5.4 Fragility Curve

Next issue is to plot fragility curves according to the methodology discussed in section 4.6. Figure 5.8 and Figure 5.9 show the fragility curves of 3 and 9-story SMRFs respectively.

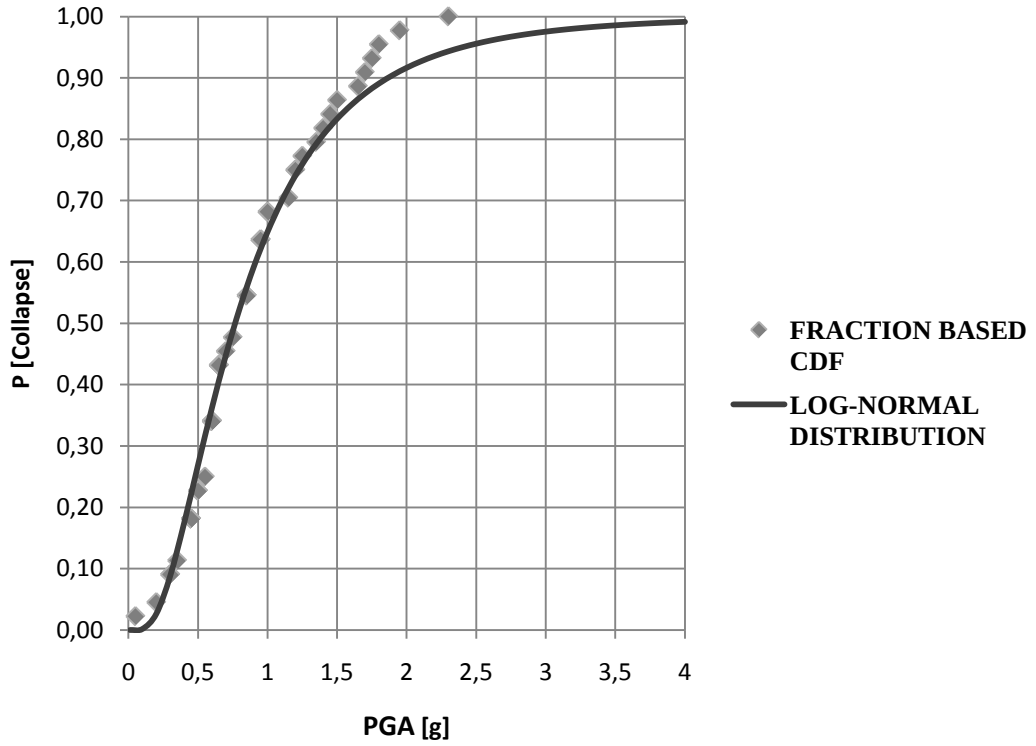

Figure 5.8: Fragility curve of 3-story SMRF

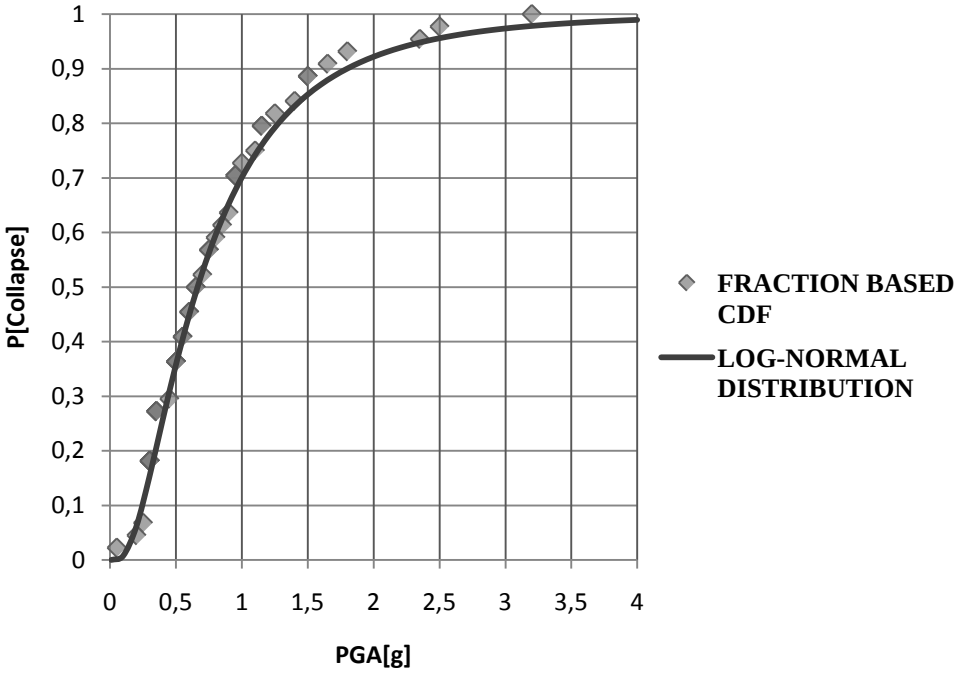

Figure 5.9: Fragility curve of 9-story SMRF

5.5 Hazard Curve

The Latitude and Longitude of Los Angeles, California where the analyzed frames are designed for are as follow:

[34° 3' 8" N - 118° 14' 34" W] or [34.05 - 118.24]

So, according to the latitude and longitude represented above, data points representing the seismic hazard curve for location of Los Angeles can be derived as it is illustrated in Figure 5.10.

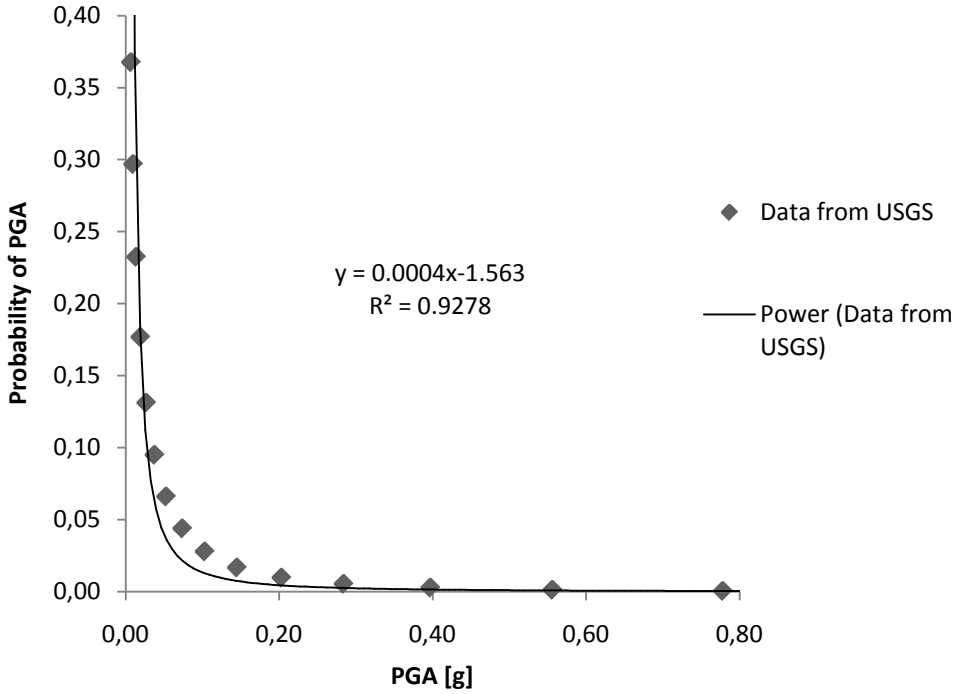

Figure 5.10: Seismic Hazard curve of Los Angeles

After fitting a line in format of Equation 4.3, the values of k_0 and k are determined.

$k_0 = 0.0004$

$k = 1.5630$

5.6 Mean Annual Frequency

Next issue is to find η_c, β_c, λ_c and finally $P[collapse]$ according to Equation 4.4 to Equation 4.7 (see Table 5.2).

Table 5.2: Mean Annual Frequency and Probability of Collapse

SMRF	η_c	β_c	λ_c	$P[Collapse]$
3-Story	0.7661	0.6943	0.001093	0.053
9-Story	0.7661	0.6771	0.001062	0.052

Chapter 6

CONCLUSIONS

Through this study, the importance of estimating collapse by the probabilistic application approach has been explained in detail and considered investigations in modeling of 3-story and 9-story steel moment resisting frames have been discussed vastly.

The modeling has been carried out by the use of OpenSEES software by using TclEditor computer programming language published by PEER center. Forty four ground motion records have been applied on the considered frames and although this number of records is more than recommended number (10 to 20), the more records will decrease the record to record (RTR) uncertainty which is the strangest characteristic of ground motions.

IDA curves have been plotted according to the applied GM records and the intensity measure of collapse of any record has been pulled out from the analyses. According to the IM_cs, fragility curves were plotted for both 3-story and 9-story SMRFs individually by IM-based method that performs with better accuracy and less upfront judgmental assumption rather than EDP-based approach [50]. The obvious similarity in fragility curves reveals that the probability of collapse under the application of specified design earthquake in codes are exactly the same of both of the considered SMRFs.

According to the probabilistic approach of calculating mean annual frequency of collapse, the probability of collapse within 50 years for 3- story and 9-story SMRFs are 5.3% and 5.2%, respectively. These values are compared with the recommended range by Haselton that is 0.7% and 7.0% [51]. According to the FEMA, design earthquake to be considered for earthquake resistant design is the earthquake that the probability of exceeding is 5% within 50 years. If a structure is designed according to the design earthquake, i.e., the structure will be in the collapse prevention limit-state, then the probability of collapse determined in this research is acceptable to be as defined by Haselton [51]. In other words, the results reveal that the SMRFs will successfully perform under the application of expected probable earthquakes that the structures should resist.

The mentioned methodology for calculating the Mean Annual Frequency discussed in Chapter 4 is a simplified method that diverts the numerical approaches and related complexities but it needs more research to prove whether this method is that accurate in comparison with the complicated numerical approaches or not.

Therefore, some future works may be recommended as below:

The similar approach can be done on new materials such as composites and fiber reinforced materials just if the cyclic behaviors are available.

The more interesting study is to apply this method on masonry structures that behave more brittle than the modern material such as steel and concrete.

As it is mentioned, the hazard curve is obtained by the USGS just for the latitude and longitude of USA. Other work that can be done by the seismologists is to find hazard data for the other parts of the world particularly for the regions that experience sever earthquakes. And, by the hazard curve data, it is possible to find the probability of collapse in the regions that has the probability of earthquake event in order to find probability of collapse of the built important structures (such as power plants, hospitals, schools and residential buildings) in that specified region whether they need strengthening or not.

REFERENCES

[1] L. F. Ibarra & H. Krawinkler. (2005). “Global Collapse of Frames under Seismic Excitations”. Stanford University. PEER 2005/06.

[2] Kaewkulchai, G. and Willamson, E.B. (2003), “Progressive collapse behavior of planar frame structures”. Proceedings of the Response of Structures to Extreme Loading Conference, Toronto, Canada.

[3] Liu, Y., Xu, L. and Grierson, D. E. (2003). “Performance of buildings under abnormal loading”. Proceedings of the Response of Structures to Extreme Loading Conference, Toronto, Canada.

[4] Jennings, P. and Husid, R. (1968). “Collapse of yielding structures during earthquakes”. Journalof the Engineering Mechanics Division, ASCE, 94, EM5, pages 1045-1065.

[5] Sun, C. K., Berg, G. V. and Hanson, R. D. (1973). “Gravity effect on single-degree inelastic systems”. Journal of Engineering Mechanics, ASCE, 99, 1, pages 183-200

[6] Bernal. D. (1987). “Amplification factors for inelastic dynamic P-Delta effects in earthquake analysis”. Earthquake Engineering & Structural Dynamics, 15, 5, July 1987, pages 635-651

[7] MacRae G. A. (1994). “P-Δ effects on single-degree-of-freedom structures in earthquakes”. Earthquake Spectra, 10, 3, Aug. 1994, pages 539-568

[8] Bernal, D. (1992). “Instability of buildings subjected to earthquakes”. Journal of Structural Engineering, 118, 8, Aug. 1992, pages 2239-2260

[9] Bernal, D. (1998). “Instability of buildings during seismic response”. Engineering Structures, 20, 4-6, Apr.-June 1998, pages 496-502

[10] Takizawa, H. and Jennings, P. (1980). “Collapse of a model for ductile reinforced concrete frames under extreme earthquake motions”. Earthquake Engineering and Structural Dynamics, 8, 1980, pages 117-144

[11] Sivaselvan, M.V., Reinhorn, A.M. (2000). “Hysteretic models for deteriorating inelasticstructures”. Journal of Engineering Mechanics, 126(6), pages 633-640

[12] Song, J. and Pincheira, J. (*2000*). “Spectral displacement demands of stiffness and strength de- grading systems”. Institute of Construction Technology, Samsung Engineering and Construction and Department of Civil and Environmental Engineering, University of Wisconsin, Madison

[13] Takizawa, H. and Jennings, P. (1980). “Collapse of a model for ductile reinforced concrete frames under extreme earthquake motions”. Earthquake Engineering and Structural Dynamics, 8, 1980, pages 117-144

[14] Aschheim, M., and Black, E. (1999). “Effects of Prior Earthquake Damage on Response of Simple Stiffness-Degrading Structures, Earthquake Spectra”. Earthquake Engineering Research Institute.

[15] Mehanny, S.S.F. and Deierlein, G.G. (2000). “Modeling of assessment of seismic performance of composite frames with reinforced concrete columns and steel beams”. John A. Blume Earthquake Engineering Research Center Report No. 135, Department of Civil Engineering, Stanford University

[16] Lee, K. and Foutch, D. A. (2001). “Performance evaluation of new steel frame buildings for seismic loads”. Earthquake Engineering and Structural Dynamics, 31, pages 653-670

[17] Jalayer, F. (2003), “Direct probabilistic seismic analysis: implementing nonlinear dynamic assessments,” PhD. Dissertation submitted to the Department of Civil Engineering, Stanford University

[18] Williamson, E.B. (2003), “Evaluation of damage and P-D effects for systems under earthquake excitation”. Journal of Structural Engineering, 129, 8, pages 1036-1046

[19] Miranda, E. and Akkar, S., (2003). “Dynamic instability of simple structural systems”. Journal of Structural Engineering, ASCE, 129(12), 1722-1726.

[20] Adam, C., and Krawinkler, H. (2003), “Large deflections of elastic-plastic frames exposed topulse-type ground motion”. Proceedings of the Response of Structures to Extreme Loading, Elsevier Science, Toronto, Canada, Aug. 3-6, 2003

[21] Yoshimura, M. and Yamanaka, N. (2000). “Ultimate limit state of RC columns”. PEER-2000/10, The Second U.S.-Japan Workshop on Performance-Based Earthquake Engineering Methodology for Reinforced Concrete Building Structures, 11-13 September, Japan, Berkeley: Pacific Earthquake Engineering Research Center, University of California, Mar. 2000, pages 313-326

[22] Sezen H. December (2002). “Seismic Behavior and Modeling of Reinforced Concrete Building Columns”. Ph.D. Dissertation. Department of Civil and Environmental Engineering. University of California, Berkeley.

[23] Moehle J. P., Elwood K. J., and Sezen H. (2002). “Gravity Load Collapse of Building Frames during Earthquakes”. ACI SP-197. Behavior and Design of Concrete Structures for Seismic Performance. American Concrete Institute. Farmington Hills, Michigan. pp. 215-238

[24] Vian, D. and Bruneau, M. (2001). “Experimental investigation of P-Delta effects to collapse during earthquakes”. Technical Report MCEER-01-0001, June 2001

[25] Kanvinde, A. M. (2003). “Methods to evaluate the dynamic stability of structures-shake table tests and nonlinear dynamic analyses”. EERI Paper Competition 2003 Winner, Proceedings of EERI Meeting, Portland, Feb. 2003

[26] Vamvatsikos, D. (2005) “Seismic performance, capacity and reliability of structures as seen through incremental dynamic analysis”. PhD Dissertation,

Department of Civil and Environmental Engineering, Stanford University, July 2005

[27] Vamvatsikos, D and Cornell, C. A. (2002). “Incremental dynamic analysis, Earthquake Engineering and structural Dynamics, 31(3): 491-514.

[28] Shome, N., and Cornell, C.A. (1999). “Probabilistic seismic demand analysis of non-linear structures”. Report No. RMS-35, Stanford University, Stanford, CA.

[29] Medina, R. (2002). “Seismic demands for nondeteriorating frame structures and their dependence on ground motions”. PhD. Dissertation submitted to the Department of Civil Engineering, Stanford University

[30] Gupta, A. and Krawinkler, H. (1999). “Seismic demands for performance evaluation of steel moment resisting frame structures”. The JohnA. Blume earthquake engineering center. Department of civil and environmental engineering, Stanford University.

[31] FEMA (2000). “State of art report on base metals and fracture”. Program to reduce the earthquake hazards of steel moment-frame resisting. Report No. FEMA-355c, Federal Emergency Management Agancy, Washington, DC.

[32] FEMA (2000). “State of art report on base metals and fracture”. Program to reduce the earthquake hazards of steel moment-frame resisting. Report No. FEMA-355a, Federal Emergency Management Agancy, Washington, DC.

[33] Filippou, Filip C., Popov, Egor P., Bertero, Vitelmo V. (1983). “Effects of bond deterioration on hysteretic behavior of reinforced concrete joints”. University of California Berkeley

[34] OpenSEES Command Language Manual: http://opensees.berkeley.edu/OpenSees/manuals/usermanual/OpenSeesCommandLanguageManual.pdf

[35] http://opensees.berkeley.edu/OpenSees/manuals/usermanual/181.htm

[36] Bernue M. et.al, (1998). “Ductile design of steel structures”, McGraw Hill book company

[37] AISC seismic provisions, ALSC- 2005

[38] Filip C., Filippou, Gregory L. Fenves. “Methods of analysis for earthquake-resistant structures”. Chapter 6 of “ earthquake engineering from engineering seismology to performance-based engineering” Edited by Bozorgnia Y. and Bertero V.

[39] Chopra A.K. (1995) “Dynamics of structures; Theory and applications to earthquake engineering”. Prentice Hall.

[40] FEMA (2000), “State of art report on base metals and fracture”. Program to reduce the earthquake hazards of steel moment-frame resisting. Report No. FEMA-355F, Federal Emergency Management Agancy, Washington, DC.

[41] Sakai J., Stephen A. M., (2004). “Analytical investigations of new methods for reducing residual displacements of reinforced concrete bridge columns”. University of California, Berkeley.

[42] Fisher, John W., Kulak, Geoffrey L. and Smith, Ian F.C. (1998). A Fatigue Primer for Structural Engineers., U.S. National Steel Bridge Alliance (NSBA), 1998.

[43] Uriz P., Mahin A.S. (2008). “Toward earthquake-resistant design of concentrically braced steel-frame structures”. Exponent-failure analysis associates Menlo Park, California and University of California, Berkeley.

[44] http://myweb.csuchico.edu/~chaselton/research/research_databases/gms_db.php

[45] Jalayer F. and Cornell C.A. (2003). “A technical framework for probability-based demand and capacity factor design (DCFD) seismic format”. California Institute of Technology and Stanford University.

[46] H. Bawker A. and J. Liberman Gerald (1972). “Engineering statistics”. Second edition. Prentice-Hall. Chapter 3.

[47] http://www.travelmath.com/city/Los+Angeles,+CA

[48] http://earthquake.usgs.gov/hazards/products/conterminous/2008/data/

[49] Naeim F. (2001), “The seismic design handbook”. Second edition, Chapter 2, Springer: 76-77

[50] F. Zareian, H. Krawinkler, L. Ibarra & D. Lignos. (2009). Basic Concepts and Performance Measures in Prediction of Collapse of Buildings under Earthquake Ground Motions. University of California- Irvine, Stanford University, Southwest Research Institute, CNWRA, San Antonio, Texas, USA.

[51] Haselton C.B. and Deierlein G.G. (2008). “Assessing seismic collapse safety of modern reinforced conceret moment-frame buildings”. Department of civil engineering, California State University, Chico and Department of civil and environmental engineering Stanford University.